ESA Climate Change Initiative – Fire_cci
D4.1.2 Product Intercomparison Report (PIR)

Project Name	ECV Fire Disturbance: Fire_cci Phase 2
Contract Nº	4000115006/15/I-NB
Issue Date	10/12/2018
Version	2.0
Author	Angelika Heil, Ioannis Bistinas
Document Ref.	Fire_cci_D4.1.2_PIR_v2.0
Document type	Public

To be cited as: Heil A., Bistinas I. (2018) ESA CCI ECV Fire Disturbance: D4.1.2. Product Intercomparison Report, version 2.0. Available at: http://www.esa-fire-cci.org/documents

Project Partners

Prime Contractor/ Scientific Lead & Project Management	UAH – University of Alcala (Spain)
Earth Observation Team	UAH – University of Alcala (Spain) EHU – University of the Basque Country (Spain) UL – University of Leicester (United Kingdom) UCL – University College London (United Kingdom) ISA – School of Agriculture, University of Lisbon (Portugal)
System Engineering	BC – Brockmann Consult (Germany)
Climate Research Group	MPIC – Max Planck Institute for Chemistry (Germany) IRD - Research Institute for Development (France) LSCE - Climate and Environmental Sciences Laboratory (France) VUA - Vrije Universiteit Amsterdam (Netherlands)

Distribution

Affiliation	Name	Address	Copies
ESA	Stephen Plummer (ESA)	stephen.plummer@esa.int	electronic copy
Project Team	Emilio Chuvieco, (UAH)	emilio.chuvieco@uah.es	electronic copy
	M. Lucrecia Pettinari (UAH)	mlucrecia.pettinari@uah.es	
	Joshua Lizundia (UAH)	joshua.lizundia@uah.es	
	Aitor Bastarrika (EHU)	aitor.bastarrika@ehu.es	
	Ekhi Roteta (EHU)	ekhi.roteta@gmail.com	
	Kevin Tansey (UL)	kjt7@leicester.ac.uk	
	Marc Padilla Parellada (UL)	mp489@leicester.ac.uk	
	James Wheeler (UL)	jemw3@leicester.ac.uk	
	Philip Lewis (UCL)	ucfalew@ucl.ac.uk	
	José Gómez Dans (UCL)	j.gomez-dans@ucl.ac.uk	
	James Brennan (UCL)	james.brennan11@ucl.ac.uk	
	Jose Miguel Pereira (ISA)	jmocpereira@gmail.com	
	Duarte Oom (ISA)	duarte.oom@gmail.com	
	Manuel Campagnolo (ISA)	mlc@isa.ulisboa.pt	
	Thomas Storm (BC)	thomas.storm@brockmann-consult.de	
	Martin Böttcher (BC)	martin.boettcher@brockmann-consult.de	
	Johannes Kaiser (MPIC)	j.kaiser@mpic.de	
	Angelika Heil (MPIC)	a.heil@mpic.de	
	Florent Mouillot (IRD)	florent.mouillot@cefe.cnrs.fr	
	Philippe Ciais (LSCE)	philippe.ciais@lsce.ipsl.fr	
	Patricia Cadule (LSCE)	patricia.cadule@lsce.ipsl.fr	
	Chao Yue (LSCE)	chaoyuejoy@gmail.com	
	Pierre Laurent (LSCE)	pierre.laurent@lsce.ipsl.fr	
	Guido van der Werf (VUA)	guido.vander.werf@vu.nl	
	Ioannis Bistinas (VUA)	i.bistinas@vu.nl	

Summary

This document describes the results of the intercomparison of MERIS Fire_cci v4.1, MODIS Fire_cci v5.0 and Fire_cci AVHRR LTDR BA products with other global BA products, according to Work Package 5100.

	Affiliation/Function	Name	Date
Prepared	MPIC VUA	Angelika Heil Ioannis Bistinas	21/11/2018
Reviewed	UAH – Project Manager	Lucrecia Pettinari	10/12/2018
Authorized	UAH - Science Leader	Emilio Chuvieco	10/12/2018
Accepted	ESA - Technical Officer	Stephen Plummer	

This document is not signed. It is provided as an electronic copy.

Document Status Sheet

Issue	Date	Details
1.0	30/03/2017	First Issue
2.0	10/12/2018	Document fully revised to address comments on CCI-FIRE-EOPS-MM-17-0044 and analysis of new products

Document Change Record

Issue	Date	Request	Location	Details
2.0	10/12/2018	MPIC-VUA	All document	Document re-written

Table of Contents

List of Tables

List of Figures

1. Executive Summary

The *Product Intercomparison Report* (PIR) describes results of the intercomparison of three satellite-based global BA products that have been generated by the ESA Fire_cci project: MODIS Fire_cci v5.0 (FireCCI50), MERIS Fire_cci v4.1 (FireCCI41), and AVHRR-LTDR Fire_cci v1.0 (FireCCILT10). These products are compared with each other and against the MODIS BA products MCD45A1, MCD64A1 (Collection 5 and 6) and GFED4s.

Intercomparison is performed globally with 0.25° spatially gridded data across 2005 to 2011 and, for selected regions, at the pixel level (250-500 m resolution). The intercomparison primarily focuses on analysing similarities and dissimilarities between different products in terms of amount of BA, observational coverage and timing of burn detection. A complementary analysis compares how the general spatial fire patterns in BA products agree with three MODIS active fire products.

The intercomparison shows that all BA products largely agree in identifying the spatial gradients and magnitude of burning in areas dominated by large savannah fires. The BA products, and particularly FireCCILT10, show stronger differences from each other in regions where smaller or infrequent fires are predominant. FireCCILT10 shows a much lower degree of spatial scattering of fire activity than all other products and also lower overall burning rates. Equatorial Asia (EQAS) exhibits the highest inter-product differences in BA rates, indicating that BA mapping in this region is still associated with large uncertainties. BA mapping across EQAS is very strongly affected by poor observational coverage which limits robust BA estimates for this region. We demonstrate that accounting for inter-product differences in the observational coverage reduces inter-product variability in BA estimates. At the pixel level and at monthly time resolution, FireCCI50 and MCD64A1 Collection 6 show low agreement in identifying individual pixels as burned, particularly outside tropical savannah regions. This mismatch can be partially attributed to differences in the timing of the burning. Pixels that are classified as burned in either product typically have a later date of burn in FireCCI50. The discrepancies in the timing of the fire event can be more than 10 days in agricultural areas.

2. Introduction

Over the past decade, several satellite-based global Burned area (BA) maps have been developed. The ESA Fire_cci project has recently generated three new global BA datasets, which are specifically designed to meet the particular requirements of climate research and modelling. They comprise MODIS Fire_cci v5.0 (FireCCI50), MERIS Fire_cci v4.1 (FireCCI41), and AVHRR-LTDR Fire_cci v1.0 (FireCCILT10). These products complement other widely used BA products such as MODIS MCD45A1 and MCD64A1 and the derived Global Fire Emission Database (GFED) products.

Each of the currently available BA products differ in the satellite sensor and/or algorithm used and in the approaches on how the uncertainties are characterized. Each

of the global BA products also has individual strengths and weaknesses (Humber et al. 2018).

Product intercomparison of space-based data records is based on comparing one geophysical variable from one product against the same entity from several independent products (e.g., produced by different algorithms or observing systems). Product intercomparison is a powerful means to indirectly validate global satellite (Zeng et al., 2015) and is an indispensable complement to direct product validation activities since the latter is limited by amount and representativity of available reference data.

The identification, characterization and understanding of the similarities and differences between different BA products are keystone in product application and for product improvement. The information gained from product intercomparison, for example, is important for fire model benchmarking (Hantson et al., 2016). Indirect product assessment by intercomparison helps to highlight regions and temporal periods where discrepancies exists which require more detailed investigation and for that reservations in the product application are advisable.

In February 2018, Humber et al. (2018) published an extensive systematic global intercomparison of the four global satellite-derived BA products. The study covers the period 2005 to 2011 and comprises the 500 m MODIS products MCD45A1 Collection 5.1 and MCD64A1 Collection 6, and the Copernicus 1 km SPOT-VGT BA product (formerly Geoland) and the MERIS Fire_cci v4.1 300 m product (FireCCI41). Humber et al. (2018) show that all BA products except for SPOT-VGT largely agree in the general spatial patterns and seasonality. SPOT-VGT detects systematically less BA globally than any other product. It is also the only product that exhibits a statistically significant downward trend in global annual BA over time. SPOT-VGT particularly misses to identify BA in the globally most dominant biomass burning regions, namely tropical Africa and Australia. Three weeks after the release of the Humber et al. (2018) study, the SPOT-VGT product was retracted from the Copernicus Global Land Service web portal to undergo further quality control analysis. This incidence illustrates the outreach of BA product intercomparison.

In the following section, we complement the Humber et al. (2018) intercomparison study of global BA products by including two recently generated Fire_cci BA products: the 300 m MODIS Fire_cci v5.0 product (FireCCI50; Chuvieco et al., 2018) and the Fire_cci 5 km AVHRR LTDR product (FireCCILT10). In addition, we include GFED4 (MCD64A1 Collection 5) and GFED4s (GFED4 with small fires), which are currently the most widely used BA products in climate applications. Furthermore, MODIS active fire products (active fire counts or "hotspots" and fire radiative energy (FRE)) are included for comparison.

In the light of the considerable quality problems of the Copernicus Land SPOT-VGT product identified and discussed in Humber et al (2018), we refrain from including this product into this global interomparison. For comprehensibleness, however, we provide a complementary SPOT-VGT product analysis in Annex 2 that is fully comparable to the analysis provided in the main document.

3. Inter-comparison of global gridded BA products: Spatial patterns

3.1. Introduction

In the following section, we inter-compare the spatial pattern of 0.25° gridded mean annual burning rates of seven global BA products listed in Table 1. In addition, three active fire products are included into the comparison. The study covers the period 2005 to 2011 where all products are temporally overlapping.

3.2. Global spatial patterns of mean annual fraction burned

All global BA and active fire products show largely similar general spatial gradients in multiyear average burning rates (Figure 1). There is widespread fire activity across the vegetated land masses. Burning rates are highest for the tropical savannah belts of Africa and Australia where more than 20% of the land is burned every year. Spatial scattering of fire activity across the land masses, however, is highest in GFED4s and in the active fire products. Here, 51 to 54% of all 0.25° land grid cells (excluding Antarctica) evidence fire activity across 2005 to 2011. Fire activity is spatially most confined in FireCCILT10, where only 26% of all land grid cells are affected. Yet, the GFED4s fire grid cells not captured by other BA products are primarily associated with very low burning rates (mean annual burned fractions below 0.01).

Globally integrated, GFED4s yields the highest annual burning rates across 2005 to 2011 (average 4.71 Mm^2) [1], followed within 8% by MCD64C6 (4.31 Mm^2). With 3.87 Mm^2, FireCCI50 yields the third largest global annual burning rates. This value is 17% lower than in GFED4s and 10% lower than in MCD64C6. Burning rates in FireCCILT10, FireCCI41, MCD64C5 and MCD45 remain between 3.41 and 3.56 Mm^2 per year, and are hence roughly 26%, 20% and 10%, respectively, lower than in GFED4, MCD64C6 and FireCCI50.

[1] Mm^2 denotes square megameter (1 Mm^2 equals 10^{12} m^2).

Table 1: Global satellite BA and active fire products included into the intercomparison. (C denoted Collection).

Product acronym	FireCCI41	FireCCI50	MCD64C5	MCD64C6	MCD45	GFED4s	FireCCILT10	GFAS	MCD14C5/ MCD14C6
Burned area product's full name	MERIS Fire_cci v4.1	MODIS Fire_cci v5.0	MCD64A1 MODIS C5.1 direct broadcast *aka* GFED4[2]	MCD64A1 MODIS C6[3]	MCD45A1 MODIS C5.1	GFED4 with small fires	AVHRR-LTDR Fire_cci v1.0	Global Fire Assimilation System v1.3	MODIS Thermal Anomalies C 5/6
Sensor	MERIS	MODIS	MODIS	MODIS	MODIS	MODIS[4]	AVHRR	MODIS	MODIS
Hybrid Algorithm[1]	MCD14C5	MCD14C6	MCD14C5	MCD14C6	No	MCD14C5	No	n.a.	n.a.
Product's spatial resolution	300 m; 0.25°	250 m; 0.25°	500 m	0.25°	500 m	0.25°	0.25°	0.1°	1 km
Temporal coverage	2005–2011	2001–2016	2000–2016	2000–ongoing	2000–2016	1997–ongoing	1982–2017	2001–ongoing	2000–ongoing
Data availability	https://geogra.uah.es/fire_cci/		ftp://fuoco.geog.umd.edu folders: /db/MCD64A1 MCD64CMQ/C6		ftp://ba1.geog.umd.edu (folder /Collection51)	http://www.globalfiredata.org/data.html	https://geogra.uah.es/fire_cci/	http://apps.ecmwf.int/datasets/data/cams-gfas/	see MCD64C5, but folders modis/C{5/6}/ mcd14ml/

[1] Burned area detection guided by 1-km MODIS active fires, either from MCD14 Collection 5 or 6.

[2] The 0.25° grid version of MCD64A1 MODIS Collection 5, known as Global Fire Emission Database (GFED) version 4 or GFED4, is available at fuoco.geog.umd.edu (folder gfed4). Only the pixel version provides information on the observational coverage. To obtain 0.25° gridded information on the observational coverage, we aggregated pixel level information to 0.25°. The aggregation of burn pixel information to gridded BA estimates yields global annual BA totals that are within 0.01% of the GFED4 estimates.

[3] The 0.25° grid version of MCD64A1 MODIS Collection 6, called Collection 6 MCD64CMQ BA climate modeling grid (CMG), was released in July 2018. MCD64A1 C6 is available at 500 m resolution from ftp://ba1.geog.umd.edu (folder /Collection6).

[4] Before 2001, BA estimated from ATSR and VIRS active fires.

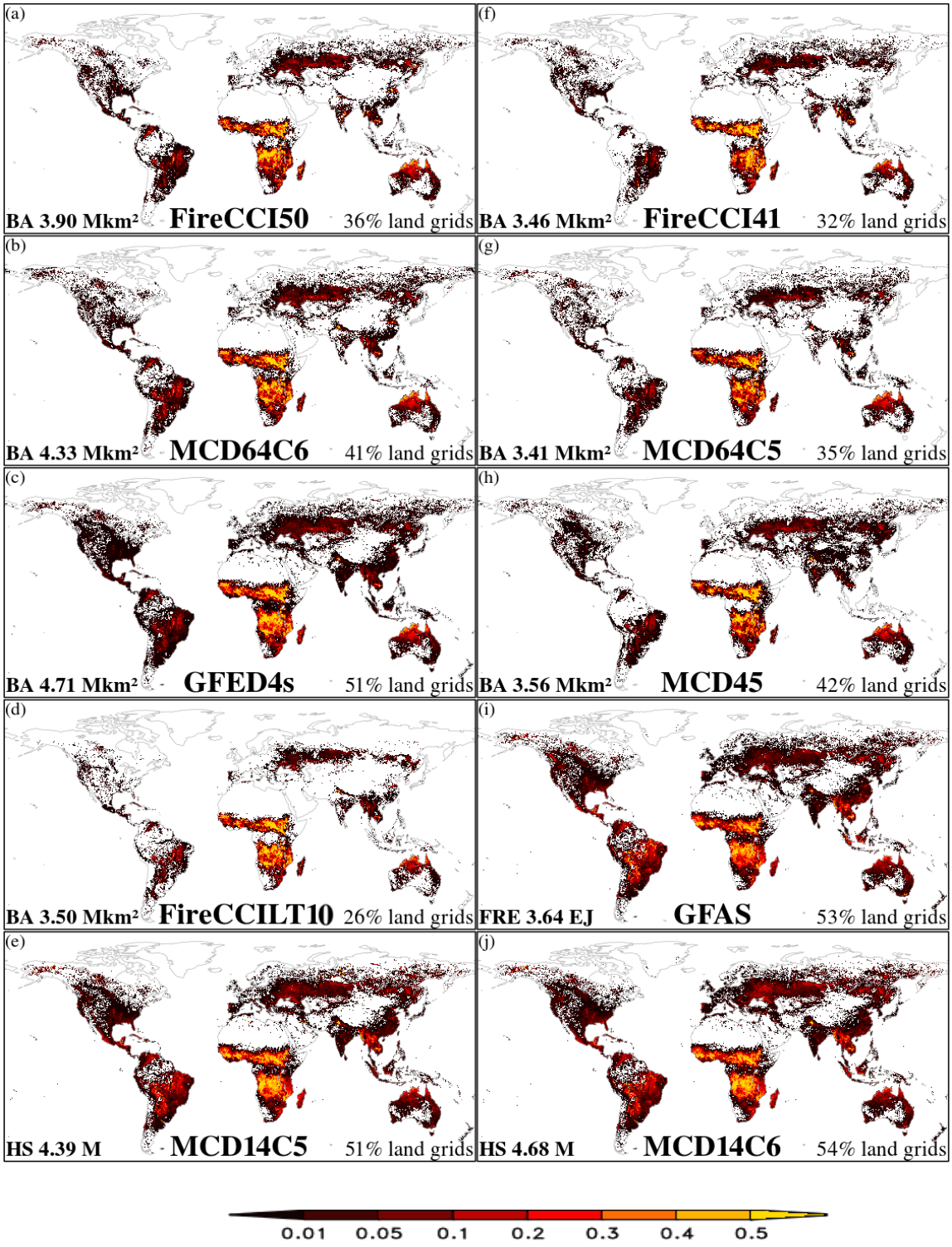

Figure 1: (a)-(d), (f)-(h) Annual burned fraction per 0.25 degree grid cell, averaged across 2005 to 2011, for different BA products. (e), (i), (j) The active fire products GFAS, MCD14C5 and MCD14C6 are displayed with a scaling factor *S* (1.60, 1.26 and 1.24, respectively) as (i) mean annual fire radiative energy (FRE) density [*SMW m^{-2}] or (e), (j) hotspot count (HS) density [*S**km^{-2}]. S targets at a comparable visual display with BA products and is calculated from the ratio of the field means of the active fire products and of FireCCI50 (only nonzero grid cells). In the left of each panel, the global total value is given (M denotes million); to the panel's right, the contribution of all nonzero 0.25° grid cells to the global number of land grid cells (excluding Antarctica) is displayed.**

3.2.1. BA by geographical regions: Regional totals

In the following section, we compare inter-product differences in BA by GFED regions (Figure 2a) and by continents (Figure 2b) using spatially aggregated statistics.

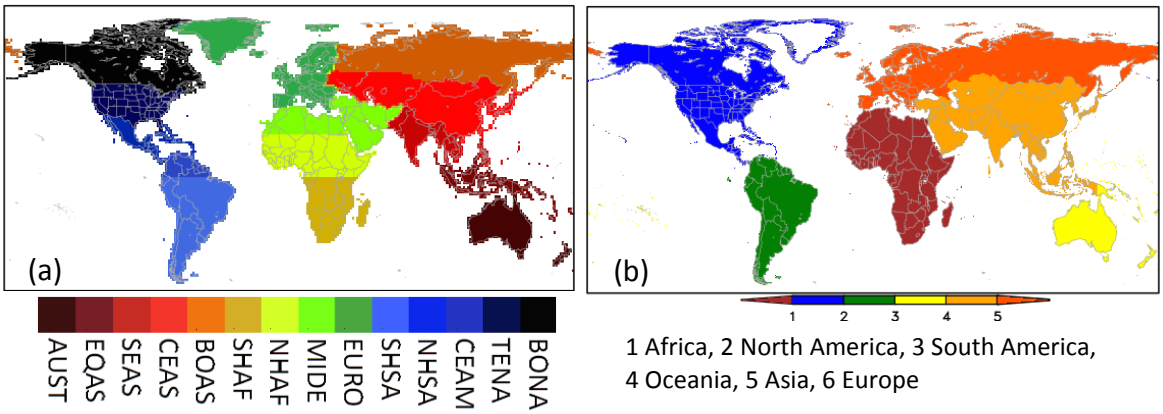

Figure 2: (a) Map of 14 GFED regions, after Giglio et al. (2010). BONA: Boreal North America, TENA: Temperate North America, CEAM: Central America, NHSA: Northern Hemisphere South America, SHSA: Southern Hemisphere South America, EURO: Europe, MIDE: Middle East, NHAF: Northern Hemisphere Africa, SHAF: Southern Hemisphere Africa, BOAS: Boreal Asia, CEAS: Central Asia, SEAS: Southeast Asia, EQAS: Equatorial Asia, AUST: Australia and New Zealand. (b) Continent map following GPWv4 national identifier map (CIESIN 2017).

All BA products attribute more than two thirds of global BA to Africa (Figure 3). Africa's contribution is highest in FireCCILT10 (77%) and lowest in FireCCI50 and MCD64C6 (both 68%). In all BA products, when ranked by continental contribution to global BA, Oceania ranks second after Africa. Europe and North America, respectively, rank five and six. The continental ranks three and four are either attributed to South America or Asia. In FireCCI50, MCD64C5/6 and FireCCILT10, South America holds rank three and Asia holds rank four while the reverse applies to all other products (Figure 3).

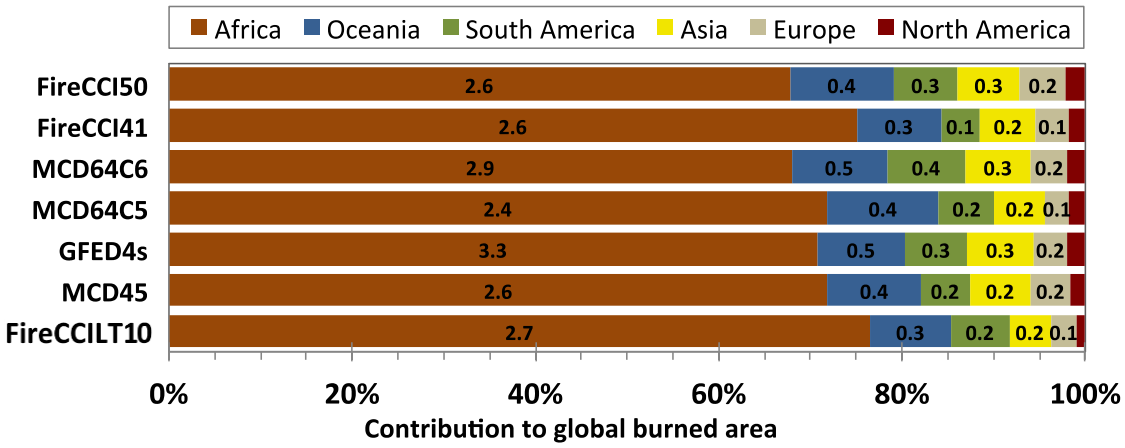

Figure 3: Continental contribution to global total BA (period 2005 to 2011) for different BA products. The bars indicate the relative contribution while data labels in the bars provide the mean annual BA [in Mm^2].

Most of the burning across Africa is attributed to Southern Hemispheric Africa (SHAF) (Figure 4, **¡Error! No se encuentra el origen de la referencia.**). Annual burning rates in SHAF differ substantially between products (between 1.44 and 1.78 Mm^2), but the differences are highly proportional to the differences in the global annual BA estimates. In all products, SHAF contributes 36 to 38% to annual global burning. The exception is FireCCILT10 where the contribution is 42%. The coefficient of determination (R^2) between SHAF and global burning rates is 89% and increases to 98% when FireCCILT10 is excluded. Accordingly, GFED4s ranks highest in SHAF burning rates, followed by MCD64C6.

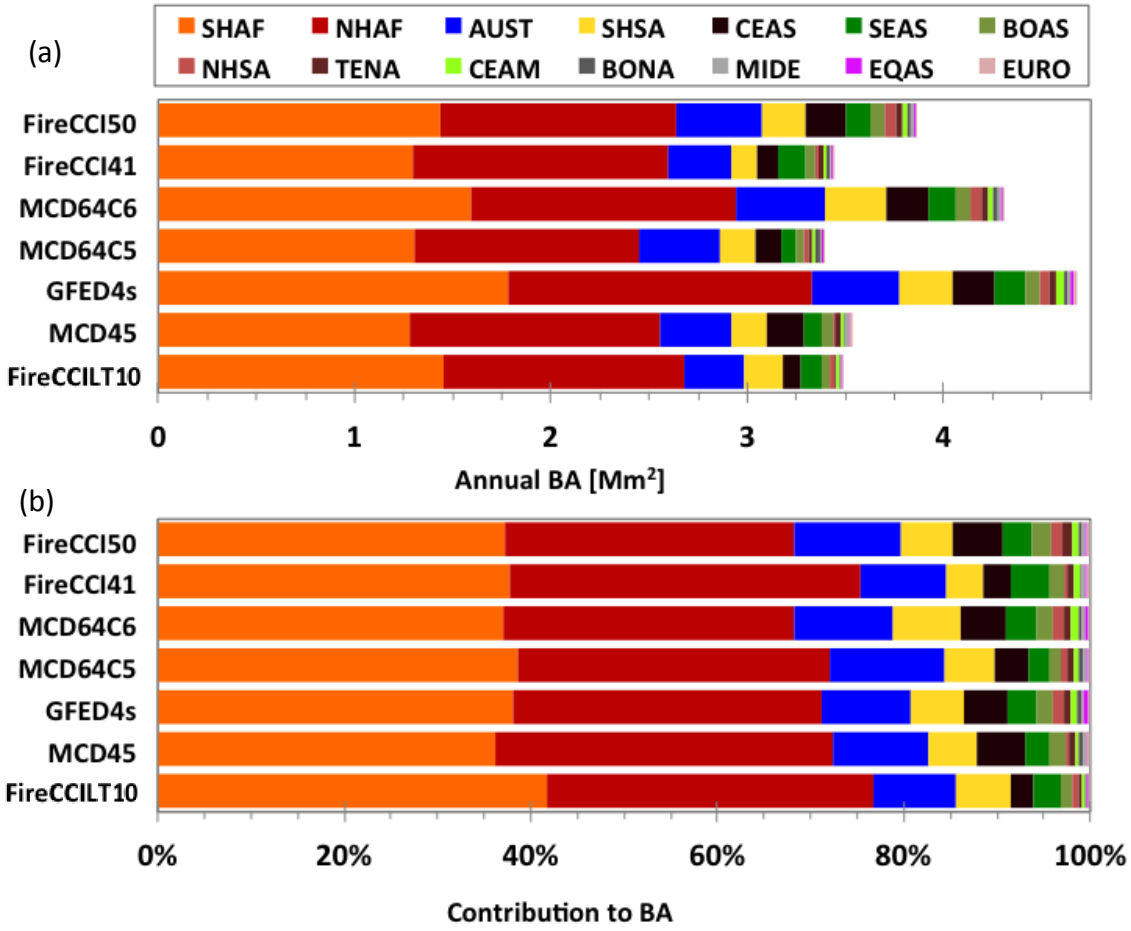

Figure 4: (a) Mean annual BA totals by GFED regions (period 2005 to 2011) for different BA products. (b) same as (a), but as relative contributions to global total BA.

In all products, BA in Northern Hemispheric Africa (NHAF) is 15 to 20% lower than in SHAF (Figure 4, Table 2). The exception is FireCCI41 and MCD45 where NHAF BA is only ~0.3% lower. NHAF's contribution to global BA is between 31 and 38%. Annual burning rates in NHAF vary between 1.14 and 1.55 Mm^2 and inter-product variability in global BA explains 70% of the variability in NHAF. Similar to SHAF, GFED4s yields the highest BA in NHAF, followed by MCD64C6.

The relative inter-product variability of the mean annual burning rates, expressed as coefficient of variation (CV), is 12% in SHAF and 10% in NHAF; hence inter-product variability in both regions is largely similar (Table 2). It is noteworthy that burning rates

in SHAF and NHAF are almost similar (less than 2% difference) within the pairs FireCCI50–FireCCILT10 and FireCC41–MCD45.

Annual burning rates in Australia (AUST) vary between 0.31 and 0.45 Mm^2 and the relative global contribution between 9 and 12%. Inter-product variance in global burning rates explains only 52% of the inter-product variance in BA in AUST. Despite strong differences in global burning rates, GFED4s, MCD64C6 and FireCCI50 yield similar and equally highest ranking BA estimates for AUST (~ 0.45 Mm^2, differences within 2%). With around 0.31 Mm^2 per year burned, FireCCI41 and FireCCILT10 yield the lowest burning rate for AUST, which is 30% less than in GFED4s, MCD64C6 and FireCCI50. Across all seven BA products, relative variability in burning rates is 15% (**¡Error! No se encuentra el origen de la referencia.**).

Table 2: Mean annual BA [in Mm2] in different GFED regions (Figure 2) and different BA products. The values refer to the period 2005 to 2011. The multi-product mean (M), standard deviation (SD) and coefficient of variation (CV) is given. "CV control" specifies the product that contributes most to the multi-product CV.

BA (mio km²)	FireCCI50	FireCCI41	MCD64C6	MCD64C5	GFED4s	MCD45	FireCCILT1	M	SD	%CV	*CV control*
Global	3.90	3.46	4.33	3.41	4.71	3.56	3.50	3.84	0.47	12	*GFED4s*
SHAF	1.44	1.30	1.60	1.31	1.78	1.28	1.46	1.45	0.17	12	*GFED4s*
NHAF	1.20	1.30	1.35	1.14	1.55	1.28	1.22	1.29	0.12	10	*GFED4s*
AUST	0.44	0.32	0.45	0.42	0.45	0.36	0.31	0.39	0.06	15	*FireCCILT1*
SHSA	0.22	0.14	0.32	0.18	0.27	0.18	0.20	0.22	0.06	26	*MCD64C6*
CEAS	0.21	0.11	0.22	0.13	0.23	0.20	0.09	0.17	0.05	32	*FireCCILT1*
SEAS	0.13	0.14	0.14	0.07	0.15	0.10	0.11	0.12	0.03	22	*MCD64C5*
BOAS	0.09	0.06	0.09	0.05	0.09	0.07	0.05	0.07	0.02	25	*MCD64C5*
NHSA	0.05	0.01	0.05	0.02	0.05	0.009	0.02	0.03	0.02	56	*MCD45*
TENA	0.04	0.03	0.03	0.02	0.03	0.03	0.01	0.03	0.008	28	*FireCCILT1*
CEAM	0.03	0.02	0.03	0.02	0.03	0.01	0.01	0.02	0.008	34	*FireCCILT1*
BONA	0.02	0.01	0.02	0.02	0.02	0.01	0.005	0.02	0.006	35	*FireCCILT1*
MIDE	0.01	0.008	0.01	0.008	0.01	0.02	0.003	0.011	0.005	42	*FireCCILT1*
EQAS	0.009	0.009	0.01	0.01	0.02	0.001	0.005	0.010	0.005	56	*MCD45*
EURO	0.01	0.01	0.01	0.006	0.01	0.01	0.005	0.010	0.003	29	*FireCCILT1*

Inter-product mean burning rate in Southern Hemispheric South America (SHSA) (0.22 Mm^2) ranks fourth in terms of global contribution, however, BA estimates across individual products vary substantially (CV=26%; range 0.14 to 0.32 Mm^2). MCD64C6 produces by far the highest regional burning rates in SHSA; BA in GFED4s, which is second highest, is already 15% lower. FireCCI41 yields the lowest estimate and is by a factor of 2.33 lower than MCD64C6 (Table 2).

All other ten GFED regions have inter-product variabilities similar to or larger than SHAF while they individually contribute less than 5% to global BA. Inter-product variability is particularly strong in Northern Hemispheric South America (NHSA) and Equatorial Asia (EQAS) with a coefficient of variation (CV) of 56%. In EQAS, annual burning rates range from 939 km^2 (MCD45) to 19,157 km^2 in GFED4s, hence vary by a factor of 20.4.

In most regions, the difference in burning rates between FireCCILT10 and the other six BA products most strongly influences the magnitude of the CV. In Africa (SHAF and NHAF), it is GFED4s (Table 2).

The large inter-product variation in individual regions indicates that BA mapping in these regions is particularly difficult, implying high uncertainties in the BA estimates. BA mapping across EQAS, for example, is particularly challenging due to the presence of water bodies, wet swamps and peat soils that tend to cause spectral confusion and which decrease the performance in discriminating between burned and unburned areas (e.g. Roy et al. 2005, Schepers et al. 2014) (Table 2). The high inter-product variation in NHSA is, as described in the next section, partially related to inter-product differences in the observational coverage. Also in EQAS, inter-product differences in the observational coverage influence inter-product differences in burning rates.

All BA products that rely on burn scars from MODIS reflectance imagery, i.e. MCD64C5, MCD64C6, GFED4s and FireCCI50, have largely similar relative distribution of BA across GFED regions (Figure 4b), despite strong differences in global total BA estimates (Figure 4a). The largest absolute difference in relative contributions in this set of products is between MCD64C5 and GFED4s in Australia. In MCD64C5, Australia contributes 12.2% to global BA while this relative contribution decreases to 9.5%, translating into a difference of 2.7%. The second largest difference is between FireCCI50 and MCD64C5 in NHAF. NHAF contribution to global BA is 33.4% in MCD64C5 and 30.8% in FireCCI50, translating into an absolute difference of 2.6%.

3.2.2. BA by geographical regions: spatial summary statistics

To quantify the inter-product spatial variability in burning rates in individual GFED regions, we calculated field statistics from the time-averaged 0.25° gridded BA products. The statistics are confined to grid cells that are classified as predominantly burnable (Figure 5).

As field statistics, we used Pearson correlation coefficient (r) and the mean absolute error (MAE). MAE is given in as percentage proportion of the grid cell area burned. r values are classified as very weak to weak (below 0.4), moderate (0.4 to 0.7), strong (0.7 to 0.9) and very strong (0.9 to 1.0).

Globally, on burnable land area, the spatial pattern of mean burning rates in FireCCI50 is highly linearly related with the patterns in the other BA products ($r \geq 0.87$, mean $r=0.89$) (Figure 6). However, correlation coefficients vary strongly for individual GFED regions. Inter-product correlation in the spatial patterns of mean burning rates is highest in AUST, followed by NHAF (r above 0.9). Inter-product spatial correlation is lowest for EQAS; the mean r across all BA products is 0.56. Of all GFED regions, EQAS exhibits also the highest relative inter-product variability in the correlation coefficients (CV of 32%) of all GFED regions. Principally, spatial correlation between FireCCI50 and active fire products ($r=0.73–0.76$) is substantially lower than the correlation between FireCCI50 and other BA products ($r \geq 0.87$).

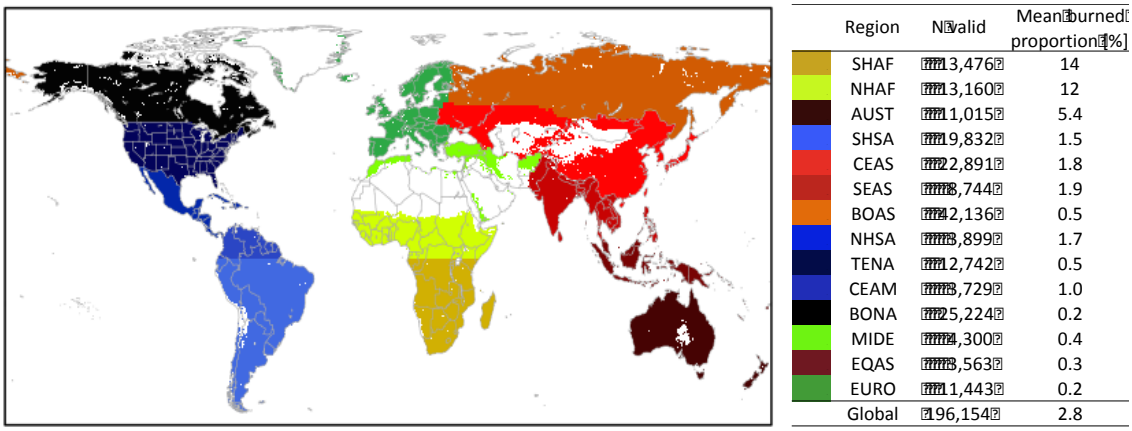

Region	N valid	Mean burned proportion [%]
SHAF	13,476	14
NHAF	13,160	12
AUST	11,015	5.4
SHSA	19,832	1.5
CEAS	22,891	1.8
SEAS	8,744	1.9
BOAS	12,136	0.5
NHSA	8,899	1.7
TENA	12,742	0.5
CEAM	8,729	1.0
BONA	25,224	0.2
MIDE	4,300	0.4
EQAS	8,563	0.3
EURO	11,443	0.2
Global	196,154	2.8

Figure 5: Predominantly burnable land mask used for field statistics using the FireCCI50 burnable area layer and a threshold of 50%. Color codes refer to the GFED region codes defined in Figure 2. The legend provides summary statistics of the number of burnable 0.25° grid cells and of the mean proportion burned per 0.25° grid cell with respect to the mean annual FireCCI50 burning rates across 2005 to 2011.

The magnitude of the inter-product MAE in the different GFED regions is largely controlled by the magnitude of the average burning rates in the individual region (values in Figure 5). The correlation coefficient *r* between FireCCI50 burning rates in the different GFED regions and the MAE, averaged across all BA products, is 0.98. The relative inter-product variability, expressed as CV, in contrast, is moderately negatively related to the burning rate (*r*=-0.48).

(a)

Region	FireCCI41	MCD64C6	MCD64C5	GFED4s	MCD45	FireCCILT1	GFAS	MCD14C5	MCD14C6	mean r (BA)	CV (BA) [%]
SHAF	.74	.81	.80	.88	.88	.83	.78	.77	.78	.82	6
NHAF	.93	.91	.90	.93	.91	.92	.84	.83	.83	.92	1
AUST	.93	.94	.94	.94	.93	.92	.73	.85	.84	.93	1
SHSA	.72	.88	.87	.88	.92	.90	.46	.53	.48	.87	8
CEAS	.78	.83	.76	.76	.78	.72	.30	.42	.58	.76	5
SEAS	.66	.65	.69	.68	.51	.70	.27	.38	.36	.68	15
BOAS	.73	.85	.68	.80	.76	.72	.66	.47	.63	.76	7
NHSA	.80	.91	.90	.92	.91	.85	.59	.57	.63	.88	5
TENA	.87	.87	.85	.87	.77	.60	.45	.67	.64	.80	12
CEAM	.42	.77	.81	.79	.71	.69	.45	.52	.53	.70	19
BONA	.80	.91	.91	.92	.80	.61	.60	.72	.71	.84	13
MIDE	.69	.76	.78	.84	.64	.65	.71	.37	.78	.76	12
EQAS	.53	.42	.42	.48	.79	.42	.18	.28	.26	.56	32
EURO	.78	.76	.68	.79	.60	.63	.46	.50	.73	.71	11
Global	.87	.89	.88	.91	.90	.88	.73	.77	.76	.89	2

r
>0.9
0.8–0.9
0.7–0.8
0.6–0.7
0.5–0.6
0.4–0.5
<0.4

(b)

Region	FireCCI41	MCD64C6	MCD64C5	GFED4s	MCD45	FireCCILT1	mean MAE	rel. MAE [%]	CV (BA) [%]
SHAF	7.5	6.9	6.8	6.5	5.1	6.3	6.5	46	11
NHAF	3.9	4.6	4.5	5.0	4.7	4.1	4.5	37	8
AUST	2.1	1.8	1.9	1.8	2.1	2.3	2.0	37	9
SHSA	1.0	1.0	0.6	0.8	0.6	0.7	0.8	54	20
CEAS	0.9	0.9	1.0	1.0	0.9	1.2	1.0	56	11
SEAS	1.4	2.0	1.6	2.1	1.9	1.7	1.8	91	14
BOAS	0.3	0.3	0.3	0.3	0.3	0.4	0.3	63	9
NHSA	1.4	0.8	1.0	1.0	1.4	1.1	1.1	65	19
TENA	0.3	0.3	0.3	0.3	0.4	0.4	0.3	65	16
CEAM	0.9	0.7	0.5	0.7	0.7	0.7	0.7	71	16
BONA	0.1	0.1	0.1	0.1	0.1	0.1	0.1	55	26
MIDE	0.2	0.3	0.2	0.3	0.5	0.3	0.3	80	31
EQAS	0.2	0.4	0.4	0.6	0.3	0.3	0.4	120	34
EURO	0.1	0.1	0.1	0.1	0.2	0.2	0.1	69	14
Global	1.3	1.3	1.3	1.3	1.2	1.3	1.3	47	3

MAE
>6.2
4.6–6.2
1.7–4.6
0.7–1.7
0.3–0.7
0.1–0.3
<0.1

Figure 6: Heatmap of inter-product field statistics with FireCCI50 mean annual BA (2005–2011) by GFED region. Predominantly unburnable grid cells are masked out. (a) Pearson's r for product-pairwise correlation, multi-product mean r and coefficient of variation (CV). The two latter are calculated only for BA products, i.e. excluding active fire products. (b) Mean absolute error (MAE) (in % of the grid cell burned) as multi-product mean MAE, relative MAE (multiproduct mean MAE divided by FireCCI50 mean proportion burned (Figure 5)), and coefficient of variation (CV). MAE color scale is using 95, 90, 75, 50, 25 and 10 field percentile values as cut-off. The number of valid grid cells by region is given in Figure 5.

Between FireCCI50 and other BA products, MAE is on average 6.5% in SHAF. FireCCI50 burning rate in SHAF, expressed as average proportion burned, is 14% (values in Figure 5). The multi-product mean MAE relative to the FireCCI50 burning rate is 46%. In regions with low burning rates such as BONA, MIDE, EQAS or EURO (< 0.4% of the vegetated land masses burning per year), multi-product mean MAE is similarly low. At the same time, the relative MAE tends to be higher than in regions with high burning rates. Across all regions, relative inter-product mean MAE and CV is highest in EQAS, pointing to the large restrictions to consistently map BA across different products in this particular region.

Figure 7 shows the results for the product-pairwise field statistics with FireCCILT10 mean burning rates as reference. Compared to the field statistics with FireCCI50 (Figure 6), the spatial BA patterns in FireCCILT10 tend to be more strongly related to those in the other BA products. The agreement in the spatial patterns is particularly pronounced in the dominant burning regions, namely SHAF, NHAF, AUST and SHSA. Reversely, in regions with lower burning rates, FireCCILT10 spatial burning patterns tend to be less associated to the patterns in other BA products. In these regions, smaller fires are more abundant (Archibald et al. 2013), which the FireCCILT10 product is limited to detect.

Figure 8 shows the cross-product field statistics with GFED4s burning rates as reference. Fields correlation coefficients between GFED4s and MCD64C5/6 are close to unity in most regions, reflecting quasi-synchronous spatial gradients in average burning rates despite differences in the absolute burning rates. Across all GFED regions, the field correlations of GFED4s with MCD64C5/6 are higher than with any other BA or active fire product. All three, GFED4s and MCD64C5/6, have been generated from the same 500 m MODIS input imagery (500 m MODIS reflectances), explaining this strong inter-dependency. Of the Fire_cci products, FireCCILT10 shows the highest spatial agreement of global mean annual burning rates with GFED4s and when quantified as linear Pearson correlation coefficient. r is 0.96, compared to 0.91 in FireCCI50 and 0.84 in FireCCI41. However, the strength of the correlation substantially decreases in regions with low mean burning rates, and is particularly low in EQAS. Also in terms of cross-product MAE, the combination of GFED4s with MCD64C5/6 yields the lowest values across all regions.

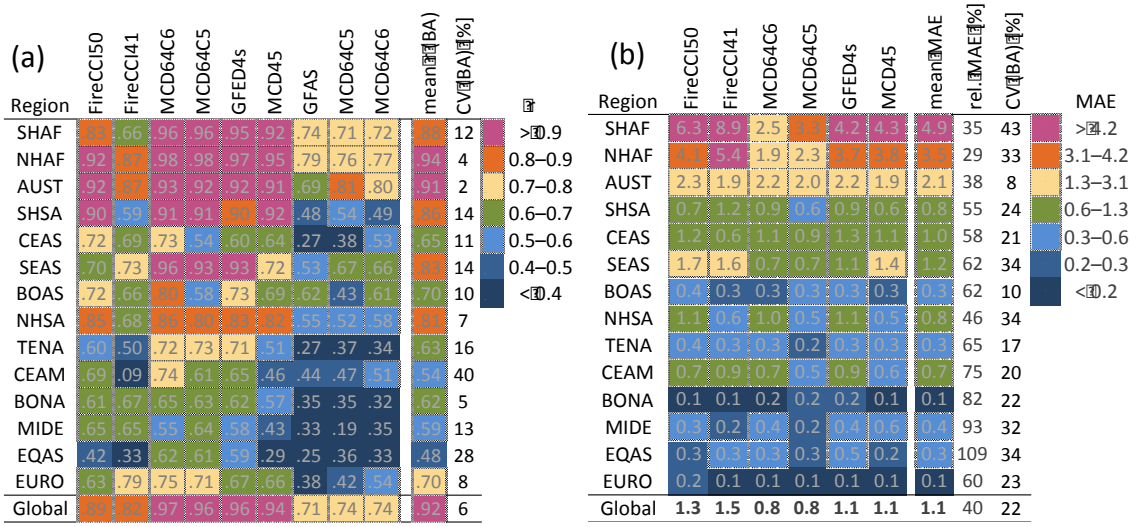

Figure 7: Same as Figure 6, but for FireCCILT10.

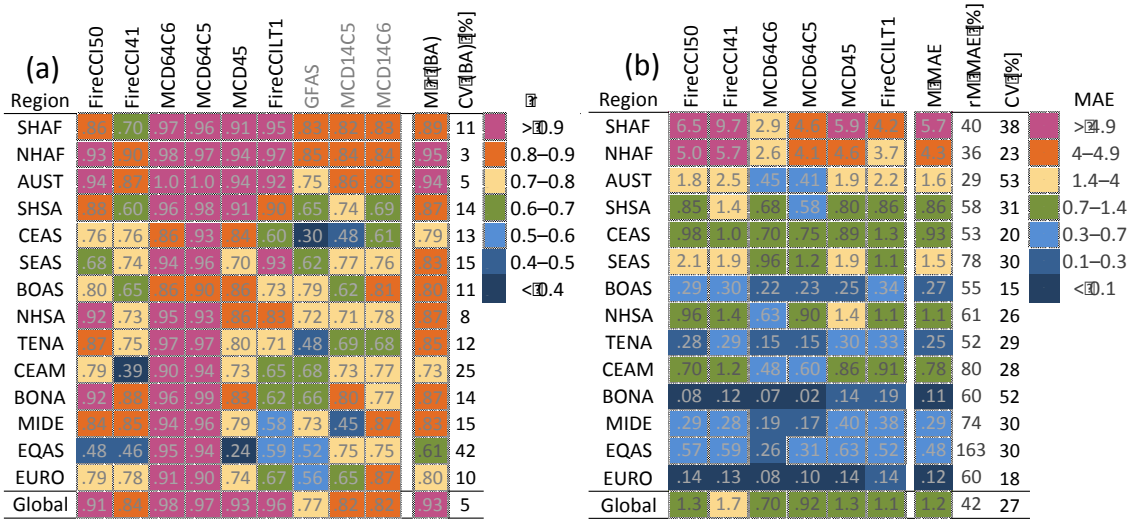

Figure 8: Same as Figure 6, but for GFED4s.

3.2.3. Spatial pattern of where which BA products yields highest burning rates

The regionally aggregated statistics do not illustrate the strong intra-regional differences in total BAs estimated by the products (Figure 9a). Across Europe, for example, GFED4s generally produces the highest BA estimates in the period 2005 to 2011 (Figure 9b). Across the Iberian Peninsula, however, and here particularly in areas with intensive agriculture, MCD45 produces the highest burning rates. In central and northern Portugal, there are additionally small regional clusters where either FireCCILT10, FireCCI41 or FireCCI50 dominate. In Eastern Europe, there are larger regional clusters where MCD64C6 or FireCCI50 yield the largest BA estimates. Interspersed are smaller clusters where FireCCILT10 or FireCCI41 dominate.

Figure 9a highlights spatially abrupt transitions between FireCCI50 and another BA product that tend to occur along the 50°N parallel across entire Eurasia and also across North America. This feature also partially occurs along the 20°S and 10°N parallels in Africa. Figure 9b-f illustrate several examples of an abrupt gradient as enlarged image detail of Figure 9a. North of the Black Sea (Figure 9b), for instance, there is a large

cluster where MCD64C6 produces highest burning rates which abruptly ends south of 50°N in order to be replaced by FireCCI50 further northwards.

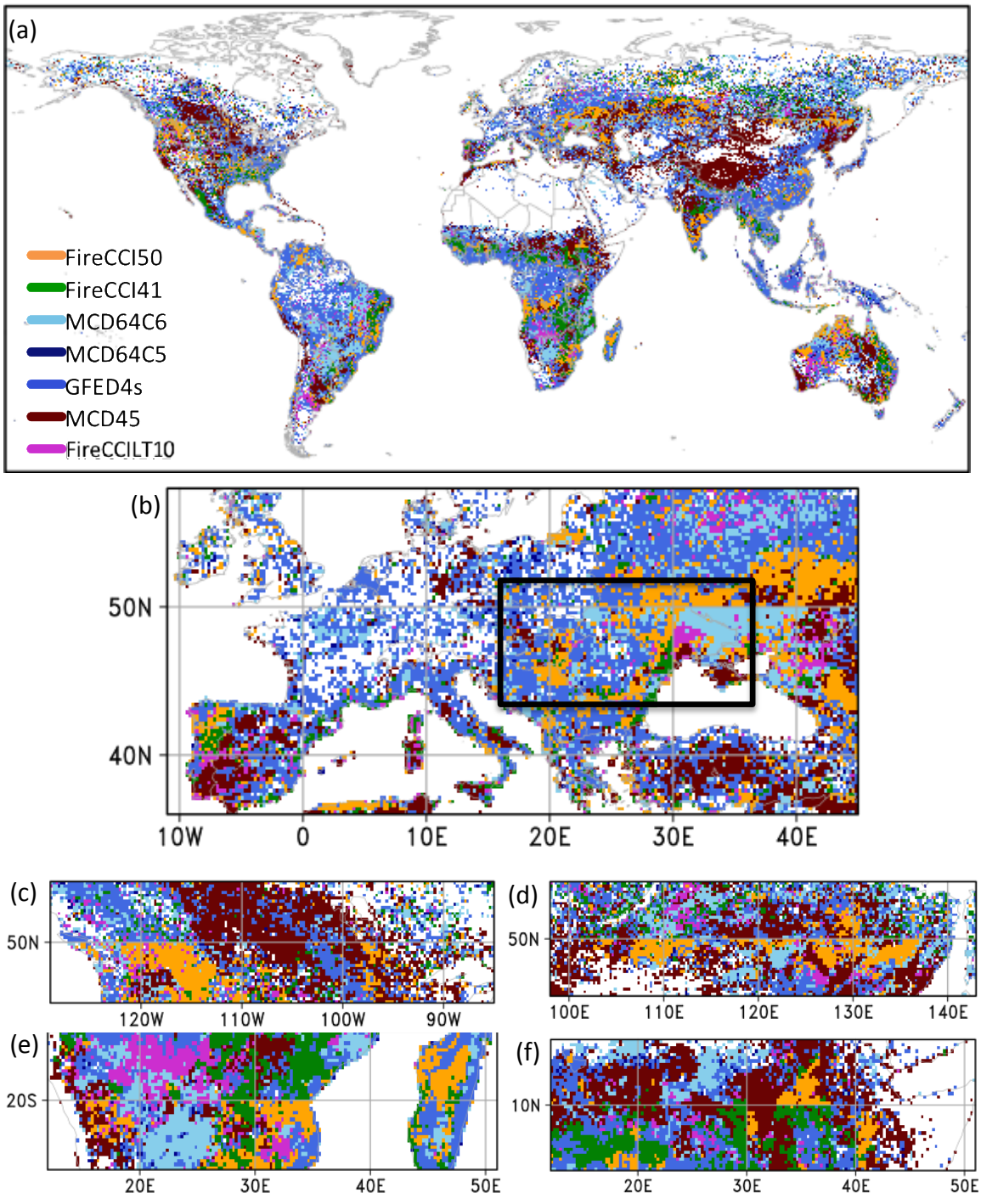

Figure 9: (a) Global 0.25° map showing the product category with the highest time-integrated BA estimate in the period 2005 to 2011. In total seven global BA products are included. White areas indicate grid cells where none of product show any burning area between 2005 and 2011. (b-f) same as (a), but enlarged for several sub-regions. The black bold frame in Figure 9 b is an extent indicator for the sub-region analyzed in more detail in Figure 10.

Humber et al. (2018) found abrupt changes in burning rates at the edges of 10°x10° tiles in FireCCI41. They interpreted this as an artefact that is related to the 10°x10° tile-wise region growing algorithm applied in the product generation. Since FireCCI50 also relies

on a tile-wise algorithm, it is likely that tiling effects cause the abrupt spatial gradients in relation to FireCCI50 as shown in Figure 9. However, the tiling effects in FireCCI50 are expected to be lower than in FireCCI41, because in FireCCI50 the threshold statistics for the burned area discrimination also consider low and high vegetation (Lizundia-Loiola et al. 2018).

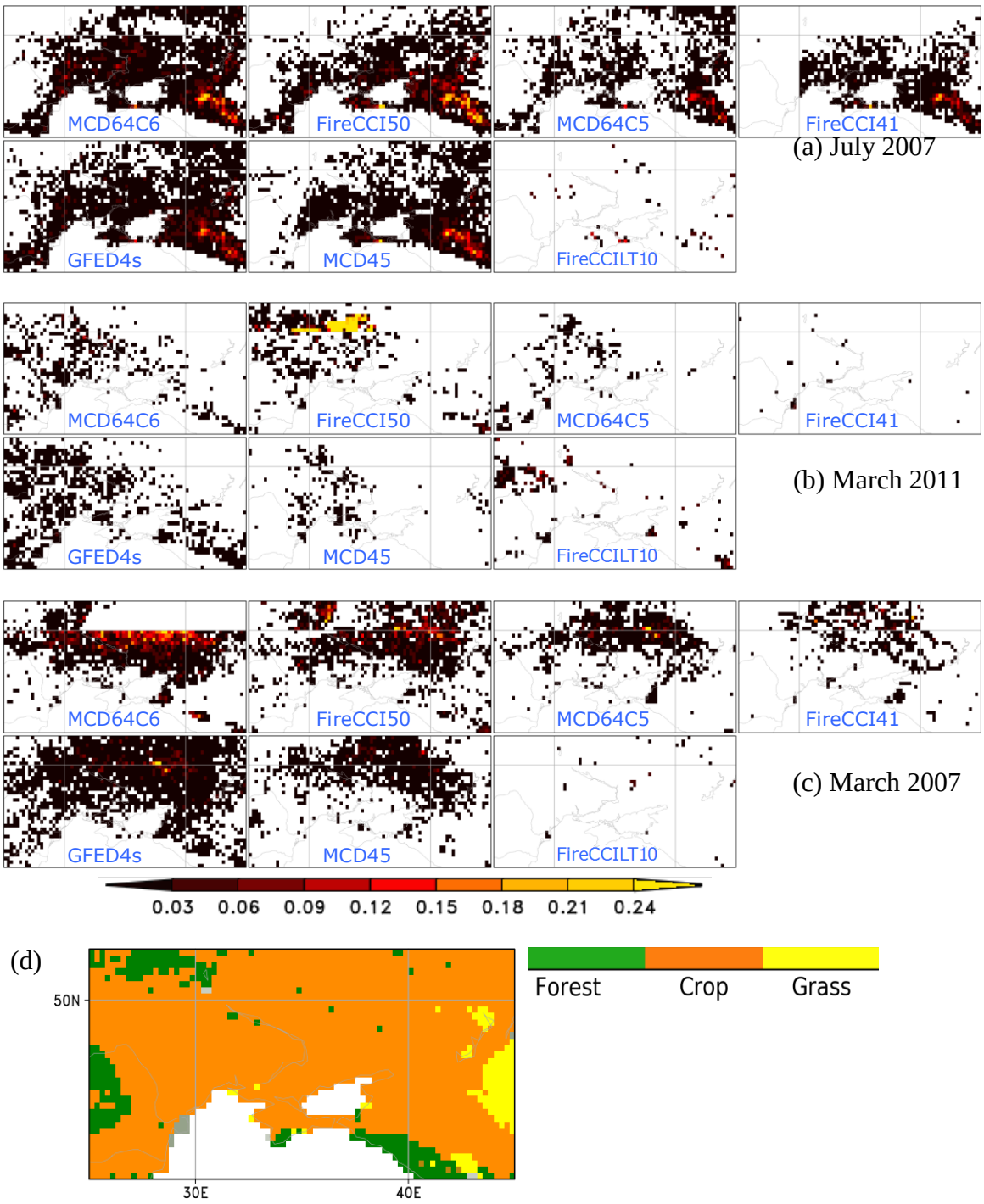

Figure 10: (a-c) Monthly burned fractions in the different BA products in a domain north of the Black Sea (region marked in Figure 9 b) and (d) dominant ESA CCI v2.0.7 land cover in 2005.

A more detailed analysis of the phenomenon for the region north of the Black Sea illustrates that there appears to be some tiling effects in FireCCI41 and FireCCI50, for

example in July 2007 (Figure 10a) and March 2011 (Figure 10b) respectively, but that there are also tiling effects in MCD64C6, for example in March 2007 (Figure 10c). Figure 10 a-c also illustrates that the abrupt spatial gradients in burning rates at the edges of 10°x10° tiles occurring in one BA product in a given month are not reflected in the other BA products. The abrupt spatial gradients are not related to changes in the vegetation cover since the dominant vegetation cover is cropland across the tile transitions (Figure 10 d).

Figure 11 illustrates the effect of abrupt gradients in the burning rates at the edges of 10°x10° tiles on inter-product differences in time-integrated burning rates across 2005 to 2011.

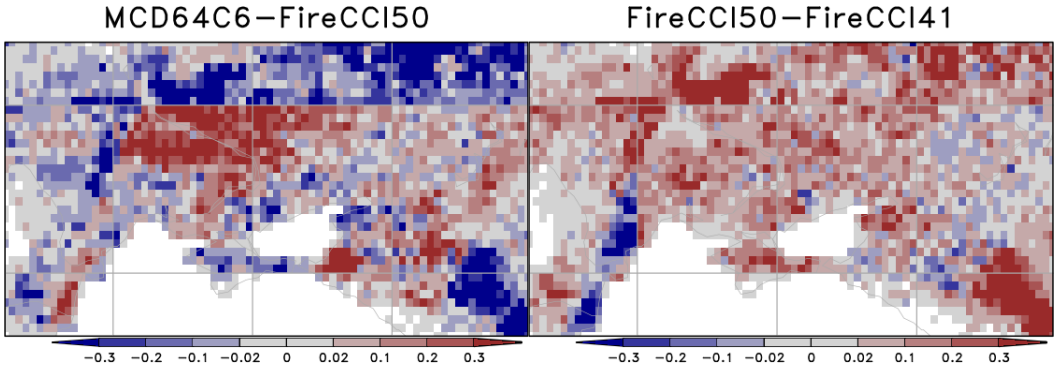

Figure 11: Absolute difference in time-integrated burned fractions (period 2005 to 2011) in the domain shown in Figure 10.

3.2.4. Influence of observational coverage on BA by geographical regions

BA mapping by satellite is strongly dependent upon the satellite's observational coverage. Some areas or individual pixels can be unmapped because the input satellite imagery is missing or corrupt, or because BA mapping is hampered due to partial, intermittent to persistent full cloud coverage.

Not considering the observational coverage can lead to various misinterpretations. For example, when not considering the observational coverage, regions and periods with low or no BA are by default interpreted as having little or no fire activity. This interpretation may be false when low or no BA values are related to poor observational coverage. It is therefore important to discriminate if the product shows no (or lower) fire activity because there was actually no (or only little) burning, or because there was no (or only poor) observational coverage. The FireCCI41 product is most strongly affected by missing satellite images and shows a strong increasing trend in the land area affected by missing tiles across 2005 to 2011, which was also observed for the MERIS leaf area index product (Tum et al. 2016).

We performed a sensitivity analysis to illustrate the effects of the observational coverage on inter-product differences in the regional mapping of BA.

For this purpose, we used the monthly fraction of observed area layer associated to (or calculated from) the FireCCI50, FireCCI41, MCD64C6, MCD64C5, MCD45 and FireCCILT10 products. Information on the observational status is generally provided with the data, either as quality flag in the pixel level product or as aggregated observational coverage layer in the grid products. However, the products apply different criteria to flag pixels as unmapped or partially unmapped or how to calculate the observational coverage for the grid level. Due to these differences, comparability of the

observational coverage information contained in or derived from various BA products is limited.

We targeted standardisation of the individual products' observational coverage information to 0.25° gridded estimates of the monthly fraction of the burnable land area that is observed (FOA) as follows:

- To convert the grid cell area to the area of burnable land per grid cell area, we used the burnable fraction layer provided with the FireCCI50 product. This layer is derived from the Land Cover CCI product.
- In FireCCI50, the fraction of observed area layer is provided as referring to the fraction of the grid cell's burnable area.
- The fraction of observed area layer provided with the FireCCI41 grid product refers to the fraction of the entire grid cell area observed which we converted to FOA.
- The fraction of observed area in the FireCCI41 and FireCCI50 grid products has biweekly resolution. Monthly information on the observational coverage can therefore be only approximated. Here, we calculate the monthly FOA from the average of the biweekly fractions.
- The 0.05° pre-release FireCCILT10 product used in this study contains a "no data" flag. For the BA classification in FireCCILT10, a random forest model is applied over a 12-month period and precedes strict data selection. A "no data" flag is applied to a pixel for all 12 months whenever a single month did not provide sufficient information for the model (personal communication, Gonzalo Otón Azofra, 28 May 2018). In FireCCILT10, "no data" values occur only north of 64° North across 2005 to 2011 and is temporally invariant, reflecting that the "no data" flag does not take into account observational constraints due to e.g. cloud or smoke cover. Nevertheless, we calculate FOA from this information.
- The monthly MCD64C6 grid product contains a layer that provides information on the unmapped spatiotemporal fraction, which was used here to deduce FOA.
- The MCD64C5 and MCD45 provide information on the observational coverage in their pixel level quality assurance layer. The layer identifies pixels that are unmapped due to insufficient valid data. The FOA at a coarser grid level can be calculated as the ratio the total number of pixels with remaining valid observations per grid cell to the total number of land pixels within this grid cell.

It is noteworthy here that the publically available GFED4 product (see Table 1), which is the default 0.25° grid product of the MCD64C5 pixel product, does not contain a data layer on the observational coverage. Also GFED4s, which is only available as grid product, does not provide such a layer. For GFED4s, we therefore assume the MCD64C5/6 observed area fraction information applies.

We created two sensitivity cases by applying thresholds for the observational quality in the monthly time series that have to be met by all BA products concurrently:

case "FOA>0.8": at least 80% of the 0.25° grid cell area is observed in a month; "quasi-fully observed land surfaces"

case "FOA>0.5": at least 50% of the 0.25° grid cell area is observed in a month; "predominantly observed land surfaces".

All gridded BA data points in the monthly time-series that do not fulfil the threshold are masked out, leading to a strong, temporally variant reduction in the total number of data points (

Figure 12).

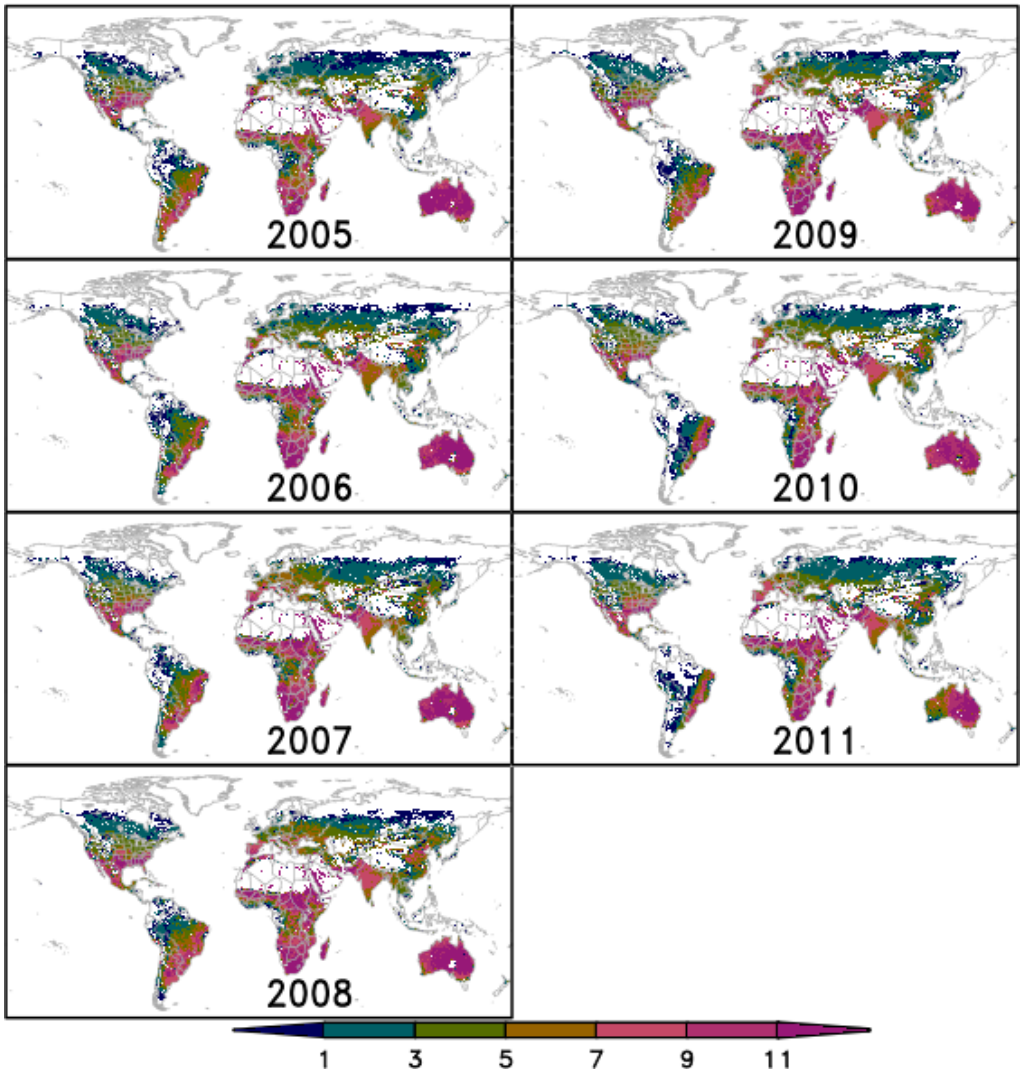

Figure 12: Annual maps of reflecting the degree of coincident quasi-fully observational coverage (FOA>0.8) in all monthly BA products [total number of months with valid observations].

In the "FOA>0.8" case with all seven BA products ("7 BA Products") included, the average proportion of land grid cells observed across 2005 to 2011 globally decreases to 24% (statistics refer to burnable land grid cells; Table 3). Most of the reduction is attributed to northern latitudes, where snow cover inhibits BA detection. In addition, cloud cover regularly inhibits detection in the tropics. In very extreme cases, such as in EQAS and NHSA, it decreases down to 1%. Across Australia, which is least affected by low observational coverage, the average proportion of land grid cells observed across 2005 to 2011 decreases to 57%. In western tropical Africa and across South America, there are substantial data gaps due to missing MERIS images in the FireCCI41 product, particularly in the years 2010 and 2011.

Excluding the FireCCI41 from the analysis ("6 BA Products") substantially reduced the loss of valid observations due to the FOA masking. In the "FOA>0.8" case, 41% of all land grid cells remain observed and in the "FOA>0.5" case 50% (Table 4). In EQAS, 11 and 24% of the land remains observed (Figure 13). However, areas prone to forest and peat fires in Sumatra remain largely unobserved.

Table 3: Multiproduct mean (M) and coefficient of variation (CV) of total BA (2005 to 2011), stratified by region and by fraction of observed area (FOA). The following seven BA ("7 BA") products are included: FireCCI50, FireCCI41, MCD64C6, MCD64C5, GFED4s, MCD45 and FireCCILT10. For the FOA classes, the corresponding multiproduct mean observational coverage is shown. Observational coverage values are calculated as time-averaged proportion of the burnable land area. The rightmost column specifies the name of the BA product that contributes most to the variance in multiproduct mean (valid for all FOA classes, except indicated otherwise).

Multiproduct Summary Statistics, Stratified by Observational Coverage

	M 7 BA Products			CV 7 BA Products [%]			M Proportion Observed [%]			CV dominating
BA [mio km²]	all FOA	FOA>0.5	FOA>0.8	all FOA	FOA>0.5	FOA>0.8	all FOA	FOA>0.5	FOA>0.8	
Global	26.87	20.72	17.54	12.1	10.0	9.8	100	85	24	GFED4s
SHAF	10.17	7.57	6.4	11.7	11.2	11.6	100	61	42	GFED4s
NHAF	9.03	8.34	7.3	9.5	9.2	9.3	100	61	44	GFED4s
AUST	2.7	2.1	1.8	14.9	12.7	11.5	100	70	57	FireCCILT1
SHSA	1.5	0.63	0.456	25.9	17.1	16.7	100	24	13	FireCCILT1 (1)
CEAS	1.2	0.81	0.69	31.7	29.8	28.4	100	31	18	FireCCILT1
SEAS	0.84	0.74	0.59	21.9	20.5	19.9	100	49	39	MCD64C5
BOAS	0.501	0.092	0.042	25.0	3.8	7.8	100	8	5	FireCCILT1 (2)
NHSA	0.223	0.020	0.006	56.5	39.5	44.7	100	3	1	MCD45
TENA	0.192	0.133	0.098	28.0	27.4	27.2	100	50	34	FireCCILT1
CEAM	0.160	0.066	0.043	33.9	34.2	39.7	100	32	18	FireCCI41 (3)
BONA	0.113	0.035	0.012	35.1	23.1	32.1	100	8	4	FireCCILT1
MIDE	0.075	0.064	0.056	42.2	42.3	42.4	100	59	46	FireCCILT1
EQAS	0.067	0.016	0.006	55.7	58.7	73.9	100	6	1	FireCCILT1 (4)
EURO	0.070	0.059	0.054	29.3	28.9	29.2	100	30	21	FireCCILT1

(1) MCD64C6 for "all FOA", (2) MCD64C5 for "all FOA", (3) FireCCILT1 for "all FOA" and FOA>0.5, (4) MCD45 for "all FOA" and FOA>0.5

Table 4: Same as Table 3, but excluding FireCCI41. The statistics therefore refer to six BA ("6 BA") products.

Multiproduct Summary Statistics, Stratified by Observational Coverage

	M 6 BA Products			CV 6 BA Products			M Proportion Land Observed			CV dominating
BA [mio km²]	all FOA	FOA>0.5	FOA>0.8	all FOA	FOA>0.5	FOA>0.8	all FOA	FOA>0.5	FOA>0.8	
Global	27.31	26.13	25.52	12.2	11.1	10.6	100	50	41	GFED4s
SHAF	10.35	10.24	10.1	11.6	11.2	10.8	100	85	72	GFED4s
NHAF	9.02	8.99	8.9	10.3	10.0	9.8	100	73	61	GFED4s
AUST	2.8	2.8	2.8	13.3	13.2	13.1	100	90	86	FireCCILT1 (1)
SHSA	1.6	1.5	1.46	21.4	18.9	17.8	100	63	52	MCD64C6
CEAS	1.2	0.96	0.86	28.7	27.4	26.4	100	40	28	FireCCILT1
SEAS	0.82	0.79	0.76	23.0	22.1	21.1	100	57	49	MCD64C5
BOAS	0.515	0.131	0.077	25.2	3.5	8.6	100	10	7	FireCCILT1
NHSA	0.246	0.138	0.100	49.3	42.3	41.1	100	34	17	FireCCI50 (1)
TENA	0.192	0.160	0.143	30.2	28.8	28.3	100	59	50	FireCCILT1 (2)
CEAM	0.164	0.153	0.138	35.5	3.6	1.8	100	81	66	FireCCILT1
BONA	0.118	0.046	0.031	34.7	27.9	27.2	100	11	8	FireCCILT1
MIDE	0.078	0.073	0.069	42.3	41.3	40.6	100	67	57	FireCCILT1
EQAS	0.067	0.034	0.020	59.8	54.0	59.6	100	24	11	MCD45
EURO	0.068	0.062	0.060	31.5	30.3	29.9	100	37	30	FireCCILT1

(1) MCD45 for "all FOA" and FOA>0.5, (2) MCD64C5 for "all FOA"

Table 3 shows that the multi-product mean global total BA across 2005 to 2011 decreases by 35 and 23% due to the FOA>0.8 and FOA>0.5 masking. This decrease is only around half the decrease in the observed global burnable land because insufficient coincident observational coverage over-proportionally affects areas in the very northern latitudes in seasons when burning rates are low compared to the burning rates in regions that are less affected by the masking. Within individual regions, however, masking strongly decreases the number BA observations. In the FOA>0.8 case, total BA calculated from the remaining valid observations decreases by 90% in boreal North America and Asia (BONA, BOAS), and in NHSA and EQAS.

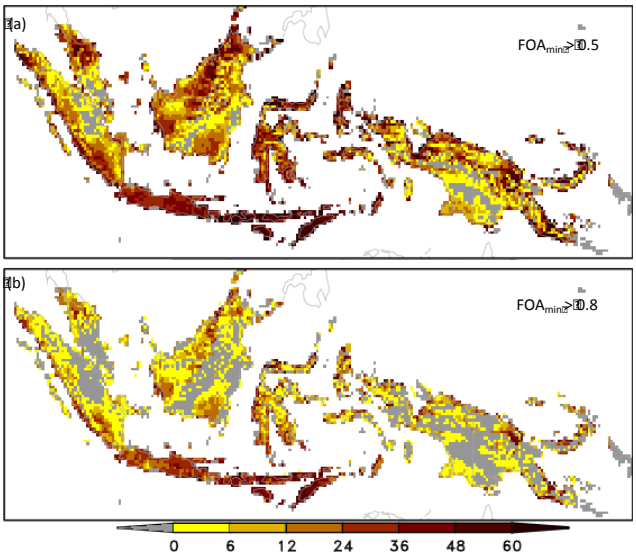

Figure 13: Total number of months with concurrent valid monthly observations across 2005 to 2011 (N_{total}=72 months) in all BA products except FireCCI41, dependent upon different minimum fraction of observed area (FOA) cutoffs: (a) FOA>0.5 and (b) FOA>0.8. Only land areas belonging to Equatorial Asia (GFED region EQAS) are color-scaled.

We analysed the relative inter-product variability, expressed as coefficient of variation (CV), in regional total BA in the remaining subset with valid observations and compare the CV values to the unmasked datasets (Table 3). The comparison shows that inter-product variability decreases when observations with insufficient observational coverage are consistently removed in all BA products. Globally, the CV decreases from 12.1 to 9.8%, which corresponds to a relative decrease of 18%. Inter-product variability in SHAF and NHAF is relatively insensitive to the masking; here the relative decrease in CV remains within 2%. Inter-product variability in SHSA decreases by 36 % and in AUST by 23%.

In some regions where the masking leads to a strong reduction in the remaining number of valid BA observations, such as in BONA, BOAS, and EQAS, the inter-product variability strongly increases by the masking because the remaining sample size is too low to obtain robust CV estimates. In addition, the masking can result in a varying regional representativity of the statistics. In the FOA>0.8 case in EQAS, for example, summary statistics over-proportionally represent fires in Java because Java is under-proportionally affected by masking and valid observations over-proportionally coincide with local fire activity. In contrast, the statistics in the FOA>0.8 case under-represent fires across Borneo and Kalimantan. The bias in regional representativity in EQAS also remains when FireCCI41 is excluded, despite the much higher number of remaining valid observations (Figure 13, Table 4). Further work will be conducted to reduce the bias in the regional representativity induced by the masking.

Yet, on the global scale and for large regions such as SHAF, NHAF, AUST and SHSA, the representativity is widely unaffected by the masking, particularly when excluding FireCCI41 (Table 4). Also in the "6 BA" scenario, masking reduces inter-product variability in burning rates in these regions. The CV related to global multi-product

mean of decreases by 13% in the FOA>0.8 case. In SHAF, while multi-product mean total BA reduces by 9% due to the masking, the CV deceases by 17%. This confirms that inter-product variability in the observational coverage substantially increased the inter-product variability in total area burned in SHSA, and should therefore be taken into consideration in product intercomparison.

4. Intercomparison of FireCCI50 and MCD64C6 BA products at the pixel level

4.1. Introduction

FireCCI50 and MCD64C6 BA are intercompared at 500 m resolution across different regions shown in Figure 14. We focussed the analysis on the period 2005 to 2011.

The goal of this analysis is to highlight the discrepancies between the two products and focuses in two aspects:

(a) the observed area of each product and where both products agree, and

(b) the difference in number of days for the day of burn (DoB) values within each cell.

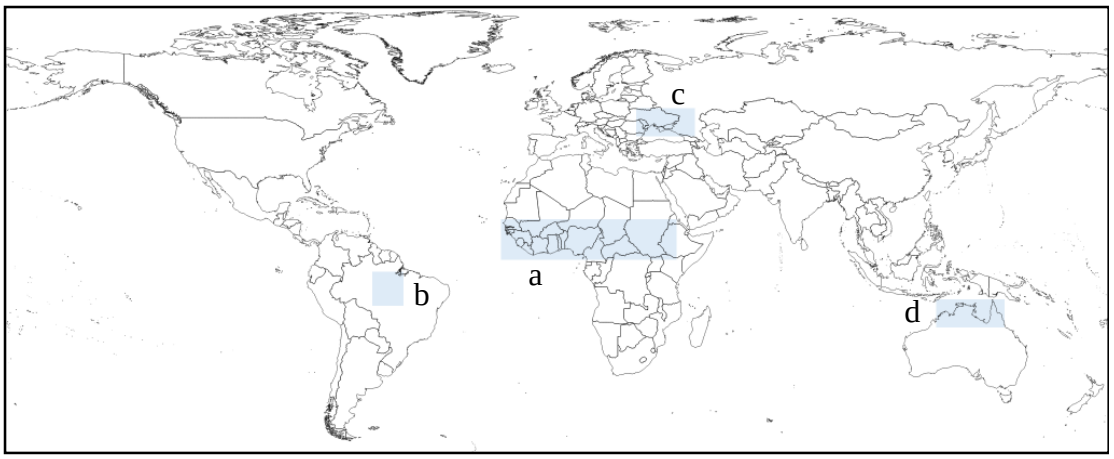

Figure 14: Case studies to focus on differences at 500 m resolution between FireCCI50 and MCD64C6. (a) Sub-Saharan north Africa, (b) South-east of the Amazon basin in Brazil, (c) Ukraine and south Russia, (d) Australian tropical savannas.

4.2. Data and methods

Product intercomparison analysis at pixel level between FireCCI50 and MCD64A1 Collection 6 (MCD64C6) requires a pre-processing in order to obtain the same spatial resolution for the monthly aggregated files. The pixel-level FireCCI50 product has pixel sizes of 250 m, whereas the MCD64C6 product has pixel sizes of 500 m. We performed the aggregation at the MCD64C6 500 m native resolution. When aggregating the FireCC50 250 m pixel information to a 500 m pixel product, we classified any 500 m pixel as burned when at least a single 250 m burned pixel falls into the 500 m pixel. Moreover, for the resampling, we took into account the most frequent value (mode) in order to assign a Day of Burn (DoB) from the pixels within the 500 m pixel. The results of the resampling keep the monthly continental tile structure of the FireCCI50 product with values of DoB. The values are Julian days (1-366) and the aggregated data have geographical coordinates using the WGS84 datum.

4.3. Results

4.3.1. Sub-Saharan Africa

In Sub-Saharan north Africa, FireCCI50 and MCD64C6 agree in classifying individual pixels as burned in around 30% of pixels classified as burned in either product (Figure 15a). Between Nigeria, Chad, Sudan and the Central African Republic, MCD64C6 detects large areas of burning that FireCCI50 fails to detect, as shown for the year 2005 in Figure 15a. Across 2005 to 2011, MCD64C6 detects 12% more BA in Sub-Saharan north Africa than FireCCI50 (annual BA 1.32 Mm^2 in MCD64C6 compared to 1.18 Mm^2 in FireCCI50; calculated from the respective grid products).

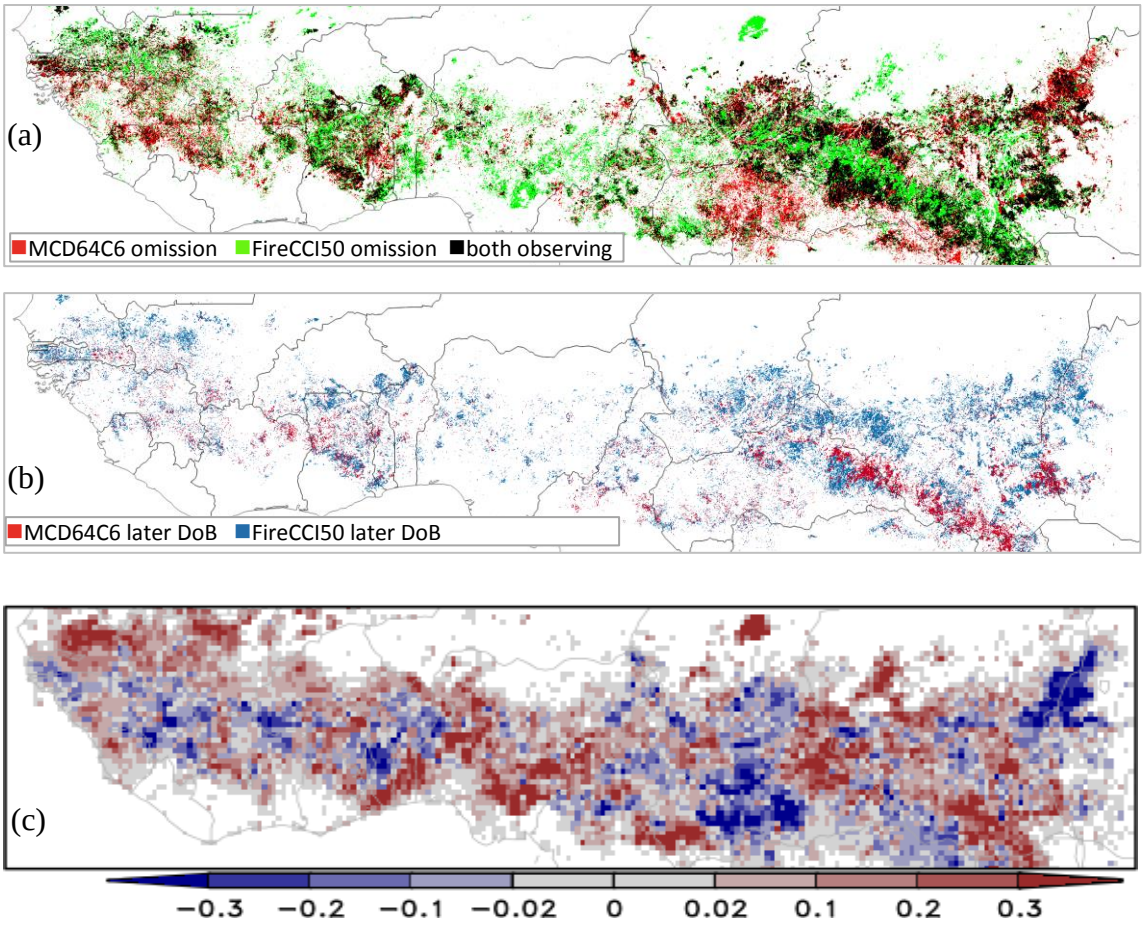

Figure 15: (a) Areas in sub-Saharan northern Africa for the year 2005 where FireCCI50 and MCD64C6 both observe and where they fail to observe. (b) Difference in the date of burn (DoB) between MCD64C6 and FireCCI50 for 2005 for "both observing" pixels. Areas where FireCCI50 has earlier DoB than MCD64C6 are shown in red. Areas where FireCCI50 has later DoB than MCD64C6 are displayed on blue. (c) For comparison, the absolute difference (MCD64C6 minus FireCCI50) in annual burned fractions in 2005 as calculated from the respective grid products is shown. Positive values indicate areas where MCD64C6 yields higher annual burning rates than FireCCI50 (reddish areas). Negative values indicate areas where FireCCI50 has higher annual burning rates than MCD64C6 (blueish areas).

In most of the globe, FireCCI50 has a Day of Burn (DoB) that is later than the ones on MCD64C6 (Figure 15 b and Figure 16), where both products agree.

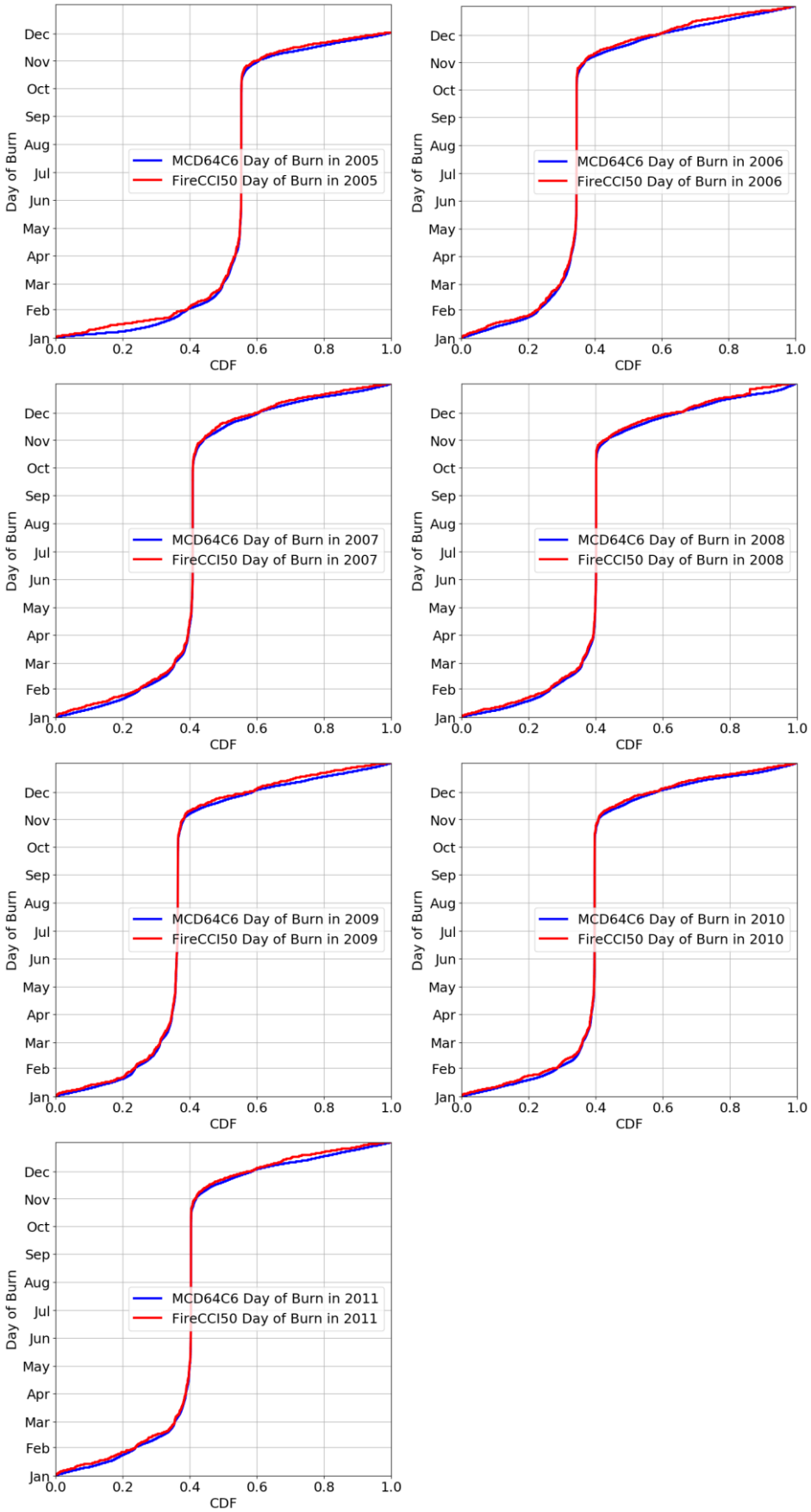

Figure 16: Cumulative Distribution Function for the differences in DoB for every year of the study period.

4.3.2. Amazon Basin (Brazil)

In the south-east of the Amazon basin (Figure 14), FireCCI50 and MCD64C6 agree in classifying individual pixels as burned in around 20 to 40% of pixels classified as burned in a given year in either product. Figure 17a shows an example of the year 2005. Across 2005 to 2011, MCD64C6 detects 39% more BA than FireCCI50 (31,842 km^2 per year in MCD64C6 compared to 22,914 km^2 in FireCCI50; calculated from the respective grid products). In the southeast of the domain, however, in an area that is dominated by shrubland, there is a large cluster where MCD64C6 fails to detect burned pixels that are detected by FireCCI50. Figure 18 illustrates that MCD64C6 is detecting more burning in active deforestation areas.

Figure 19 shows that the differences in DoB between FireCCI50 and MCD64C6 are higher than in the Sub-Saharan Africa study area (section 4.3.1). Burn date detection in FireCCI50 can be up to 8 days later than in MCD64C6

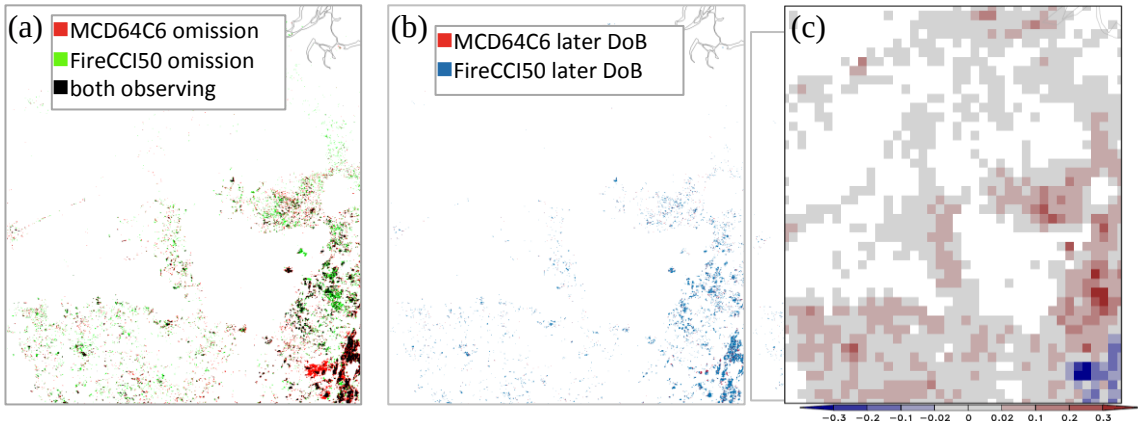

Figure 17: Same as Figure 15, but for areas in South-east of the Amazon basin in Brazil for the year 2005.

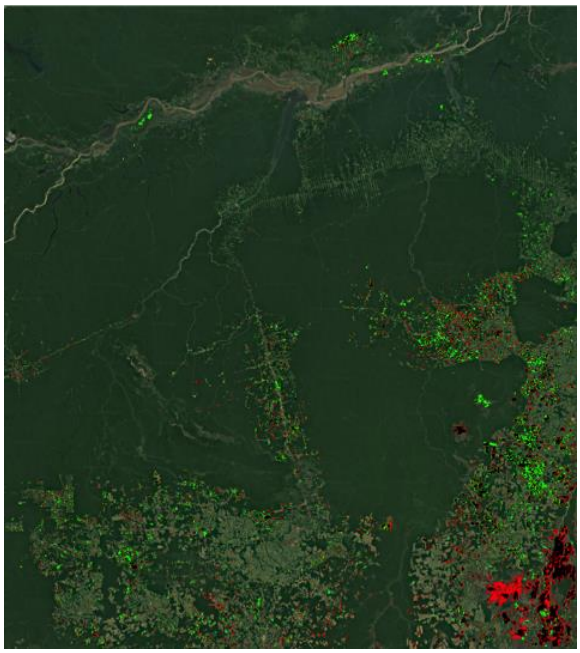

Figure 18: After Figure 17a, an example area of South-east of the Amazon basin in Brazil for the year 2005 superimposed to the Landsat 8 image. The figure highlights omissions from MCD64C6 (red overlay) in dominantly deforested areas to the southeast. It also highlights omissions in the FireCCI50 product (light green overlay) at the forest edges where active deforestation is ongoing.

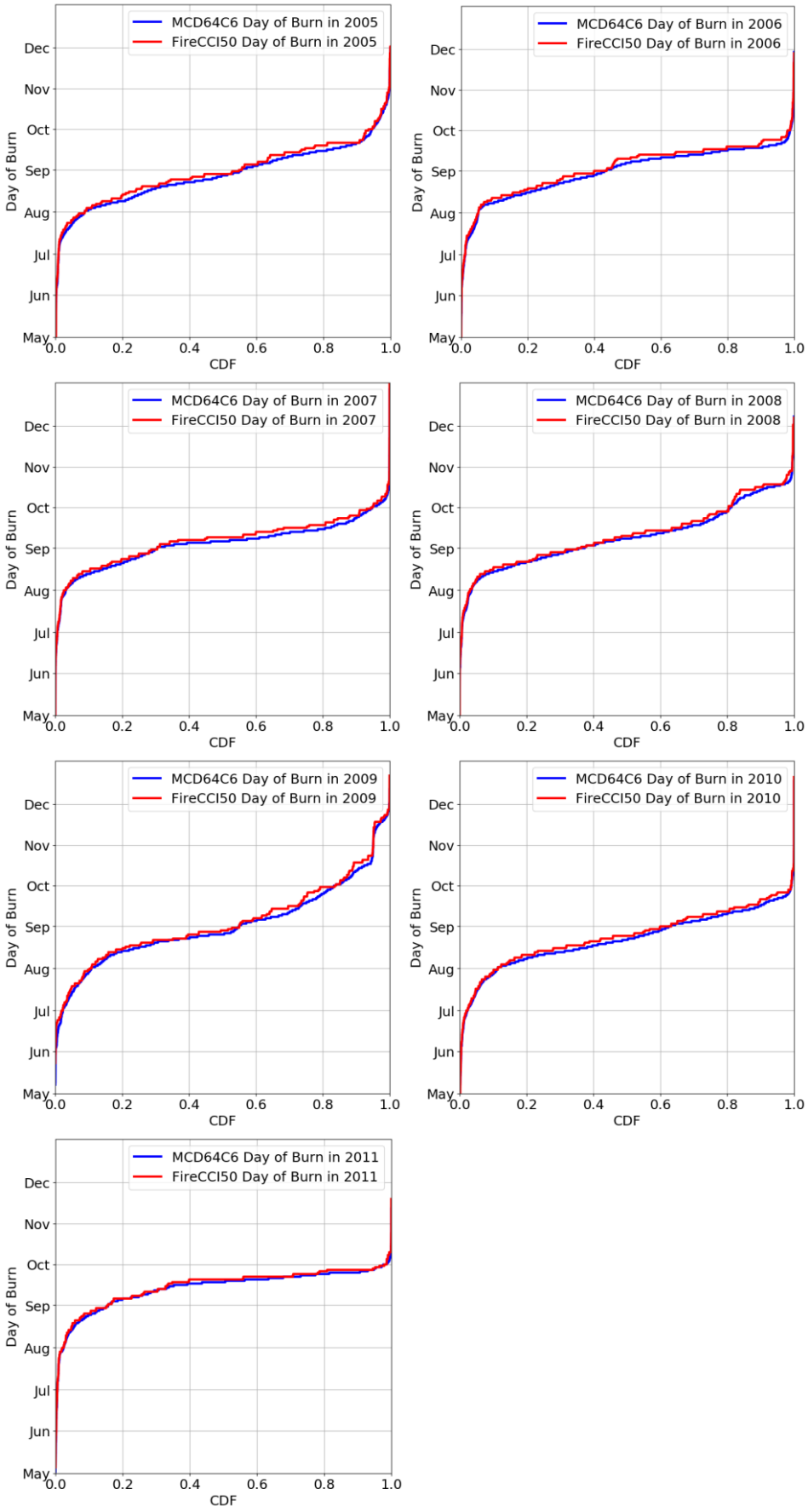

Figure 19: Cumulative Distribution Function for the differences in DoB for every year of the study period in South-east of the Amazon basin in Brazil.

4.3.3. Ukraine

In the croplands of Ukraine and southern Russia, FireCCI50 and MCD64C6 show the lowest agreement in classifying pixels as burned. The majority of the fires in this area are small agricultural fires. Depending on the year, FireCCI50 detects between 13% less (year 2009) to 94% more (year 2011) burned area than MCD64C6. Figure 18 shows for the year 2005 where both products agree or disagree in mapping burned pixels. Across the years 2005 to 2011, less than 10% of all pixels classified as burned are identified in both products. The FireCCI50 burn date in these "both observing" pixels is more than 10 days later than MCD64C6 (Figure 19), which is the DoB highest difference of all regions analysed in this report.

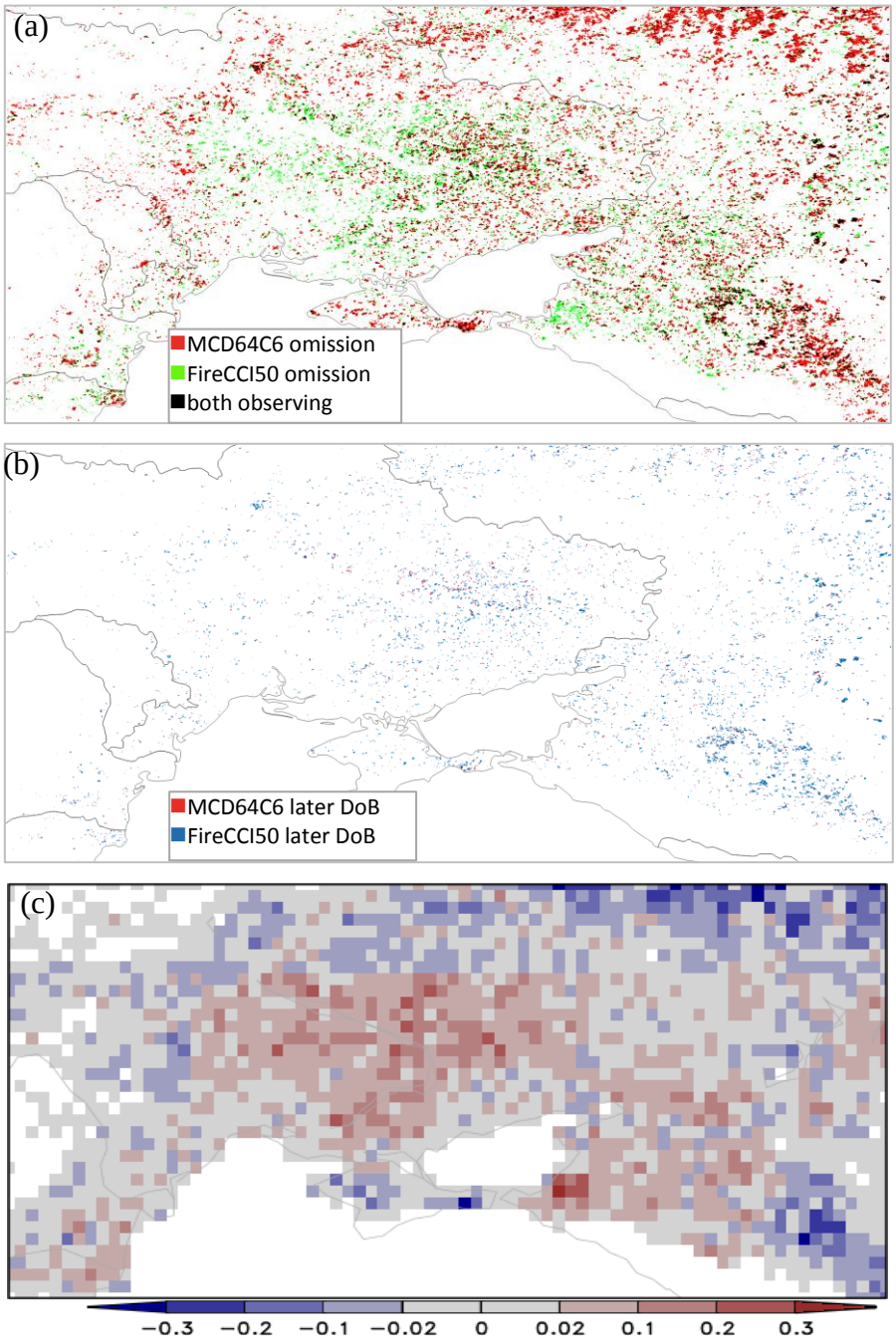

Figure 20: Same as Figure 15, but for areas in Ukraine and south Russia for the year 2005. Total BA in 2005 in MCD64C6 is 9% higher than in FireCCI50.

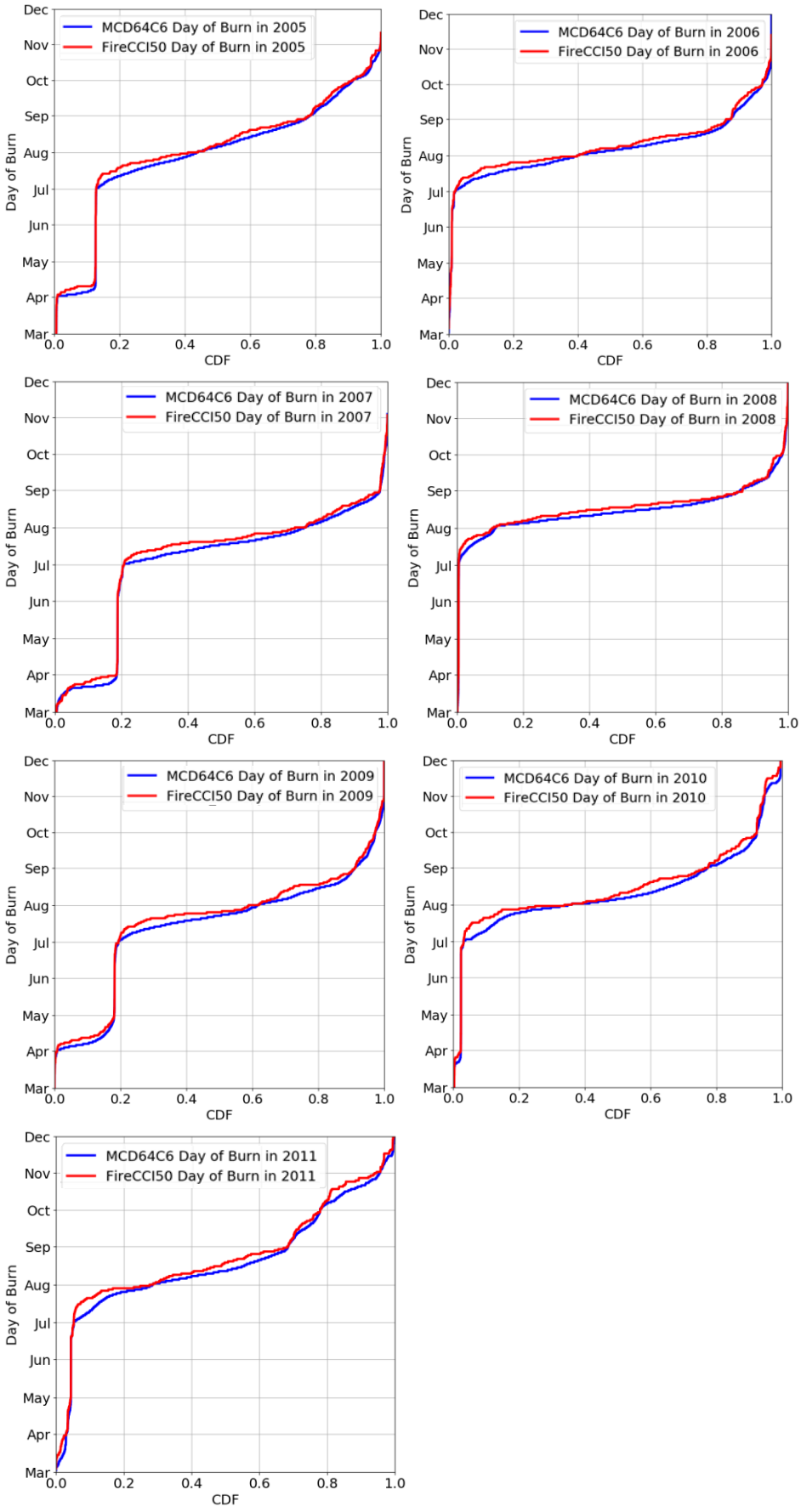

Figure 21: Cumulative Distribution Function for the differences in DoB for every year of the study period in Ukraine and south Russia.

4.3.4. Australia

The Australian tropical savannas are characterized by large wildfires that can burn multiple days. In this region, FireCCI50 and MCD64C6 show relative high agreement in mapping pixels as burned (typically around 40% of all pixels classified as burned agree) (Figure 22). The area burned across 2005 to 2011 agrees within 3% in both products. While FireCCI50 has a later DoB than MCD64C6, the absolute difference in DoB is the smallest of all regions analysed in this report (Figure 23).

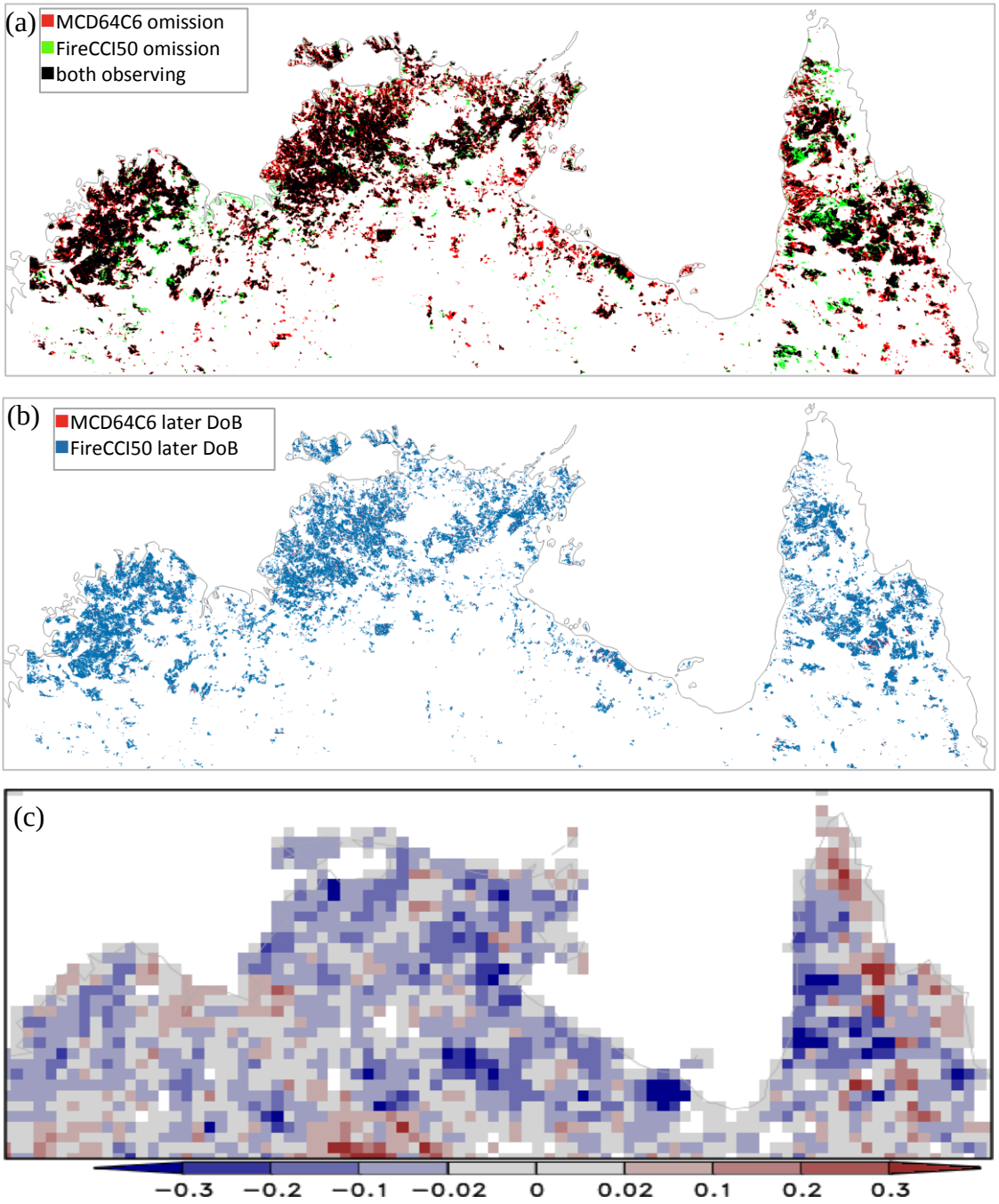

Figure 22: Same as Figure 15, but for Australian tropical savannas for the year 2005.

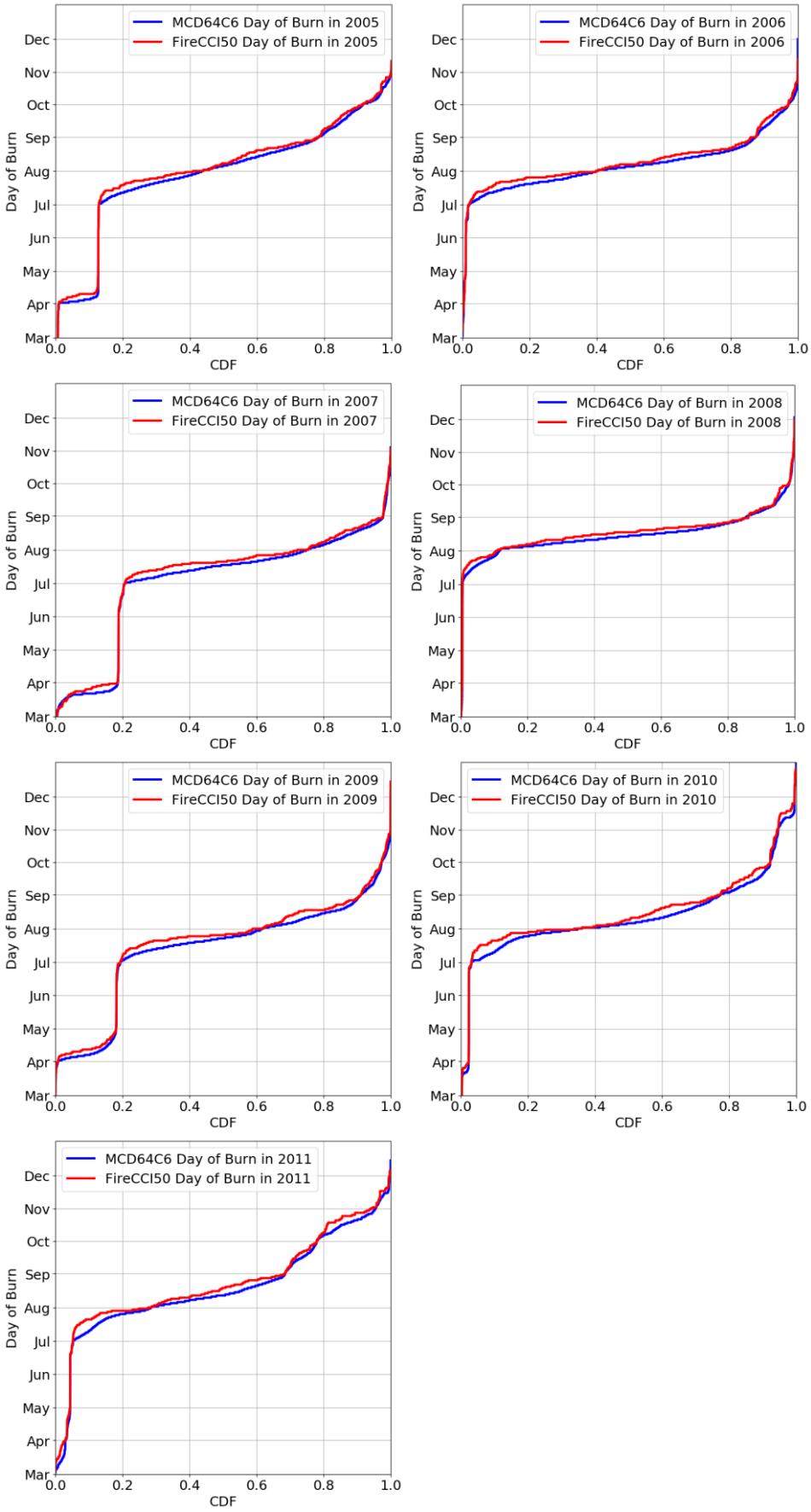

Figure 23: Cumulative Distribution Function for the differences in DoB for every year of the study period in Australian tropical savannas.

4.4. Discussion and conclusions

The intercomparison of FireCCI50 and MCD64A1 Collection 6 (MCD64C6) BA at the pixel level shows that both products have the highest agreement in identifying burned pixels in savannahs where fire sizes are large. The intercomparison demonstrates large discrepancies in areas with fragmented and smaller fires and areas with seemingly higher tree cover. In areas with small agricultural fires and in areas with higher tree cover, FireCCI50 can have considerable omissions.

The date of burn (DoB) in FireCCI50 is almost always later than in MCD64C6. The discrepancies in timing of the fire event (DoB) can be more than 10 days in agricultural areas. The differences in the DoB are probably related to satellite overpass and coverage effects since the FireCCI50 product relies on the Terra platform alone while MCD64C6 uses information from Terra and Aqua. In addition, FireCCI50 and MCD64C6 differ in the composite techniques used.

Differences in the timing of the burning event can be vital for the calculation of fire-induced emissions since fuel conditions are highly time-variant and different fuel conditions can lead to higher or lower emission estimates.

5. Synthesis conclusions

We intercompared seven global BA products across 2005 to 2011 in view of the amount of burning, spatial patterns, observational coverage and timing of burn detection.

Annual global burning rates in the individual products range between 3.41 and 4.7 Mm^2. GFED4s yields the highest rate, followed by MCD64C6 (4.3 Mm^2) and FireCCI50 (3.9 km^2). Burning rates in FireCCILT10, FireCCI41, MCD64C5 and MCD45 are between 3.41 and 3.56 Mm^2. All products attribute more than two third of global BA to Africa, and here most of it to Southern Hemispheric Africa (SHAF).

Inter-product differences in regional BA totals are largely proportional to the differences in the global BA estimates, reflecting consistency in the regional attribution of burning between products. It may also reflect the common dependency of the products from MODIS reflectance or active fire information. FireCCILT10 is the only product included into this intercomparison that is not directly dependent upon MODIS information.

Principally, FireCCILT10 closely reproduces the MCD64-based BA products MCD64C5/6 and GFED4s in terms of similar spatial gradients and magnitude of burning in areas dominated by large savannah fires. In contrast, FireCCILT10 strongly differs from all other products in regions where smaller or infrequent fires are predominant. In those cases, FireCCILT10 shows a much lower degree of spatial scattering and of total burning rates. For example, FireCCILT10 captures burning in 26% of all 0.25° resolved land grid cells globally. The spatial scattering is distinctively higher in all other BA products and even more than twice as high in GFED4s and in active fire products. The fire activity not captured by FireCCILT10 contributes little to global BA, since these fires are typically small or infrequent. Mapping of small fires in FireCCILT10 is very limited by the coarse sensor spatial resolution, which is much coarser than the resolution of the sensors used in the other BA products. The omission

of these fires, however, restricts the products' usability for various global climate applications, such as fire regime analysis (Archibald et al. 2013) or global fire model benchmarking (Hantson et al. 2016) where regions with small or infrequent fires are attributed an equally informative value as large and frequent fires.

Equatorial Asia (EQAS) exhibits the highest inter-product differences in BA rates. This indicates that BA mapping in this region is still associated with large uncertainties. BA mapping across EQAS is very strongly affected by poor observational coverage which limits robust BA estimates for this region. Fire emissions from EQAS are of particular relevance for global carbon cycle modelling since in extreme years, such as in 1997, it is estimated that carbon released by fires in EQAS may contribute up to 37% to total fire-related carbon emissions (van der Werf et al. 2017). Narrowing down the uncertainties in BA estimates for EQAS would therefore be of key value for global carbon cycle studies.

We demonstrate that inter-product variability in the observational coverage influences the inter-product variability in BA estimates. In Southern Hemisphere South America, for example, consistent masking of insufficiently observed data points in all BA products substantially reduces the inter-product variability in the BA estimates. It shows that observational coverage needs to be taken into consideration in product intercomparison. Unfortunately, information on the observational coverage is still inconsistent between products; the development of standardised observational coverage data layers in gridded global BA products would be desirable.

A pixel-level analysis reveals that FireCCI50 tends to detect fires later than MCD64C6. This difference in the date of burn (DoB) is particularly pronounced in agricultural areas, where it can be more than 10 days. The differences in the DoB detection have various implications for science applications. One implication is that fire emission estimates that combine temporally overlapping information of BA and fuel conditions may use incorrect fuel conditions because of unaccounted temporal errors in the DoB.

Both, the grid level and the pixel analysis, pinpoint that FireCCI50 and MCD64C6 show highest agreement in areas dominated by savannah fires. In the savannah region of Australia, FireCCI50 consistently detects higher burning rates than MCD64C6. The grid level and the pixel analysis also both show that BA estimates largely disagree in areas with small agricultural fires and in areas characterised by fragmented vegetation cover, such as the tropical deforestation areas in South America.

In certain regions and periods, FireCCI41 BA exhibits abrupt spatial gradients along the edges of the 10°x10° processing tiles. Also FireCCI50 and MCD64C6 appear to be affected by tiling effect, although to a smaller extend than in FireCCI41. Tiling artefacts are, for example, apparent at the 50°N parallel across Eurasia and Canada. These spatial inconsistencies may substantially reduce the usability of the products for regional studies and should be addressed with priority in future product releases.

6. References

Archibald, S., Lehmann, C., Gomez-Dans, J., and Bradstock, R.: Defining pyromes and global syndromes of fire regimes. Proceedings Of The National Academy Of Sciences, 110(16), 6442-6447. doi: 10.1073/pnas.1211466110, 2013.

Center for International Earth Science Information Network - CIESIN - Columbia University. 2017. Gridded Population of the World, Version 4 (GPWv4): National Identifier Grid, Revision 10. Palisades, NY: NASA Socioeconomic Data and Applications Center (SEDAC). https://doi.org/10.7927/H4T72FDB. Accessed 26 August 2018.

Chuvieco, E., Lizundia-Loiola, J., Pettinari, M. L., Ramo, R., Padilla, M., Tansey, K., Mouillot, F., Laurent, P., Storm, T., Heil, A., and Plummer, S.: Generation and analysis of a new global BA product based on MODIS 250 m reflectance bands and thermal anomalies, Earth System Science Data 10, 2015-2031, https://doi.org/10.5194/essd-10-2015-2018, 2018.

Giglio, L., J. T. Randerson, G. R. van der Werf, P. S. Kasibhatla, G. J. Collatz, D. C. Morton, and R. S. Defries, Assessing variability and long- term trends in burned area by merging multiple satellite fire products, Biogeosciences, 7, 1171–1186, doi: 10.5194/bg- 7- 1171- 2010, 2010

Hantson, S., Arneth, A., Harrison, S. P., Kelley, D. I., Prentice, I. C., Rabin, S. S., Archibald, S., Mouillot, F., Arnold, S. R., Artaxo, P., Bachelet, D., Ciais, P., Forrest, M., Friedlingstein, P., Hickler, T., Kaplan, J. O., Kloster, S., Knorr, W., Lasslop, G., Li, F., Mangeon, S., Melton, J. R., Meyn, A., Sitch, S., Spessa, A., van der Werf, G. R., Voulgarakis, A., and Yue, C.: The status and challenge of global fire modelling, Biogeosciences, 13, 3359-3375, https://doi.org/10.5194/bg-13-3359-2016, 2016.

Humber, M.L., Boschetti, L., Giglio, L., and Justice, C.O.: Spatial and temporal intercomparison of four global BA products. International Journal of Digital Earth, 1-25, 2018.

Lizundia-Loiola J., Pettinari M.L., Chuvieco E., Storm T., Gómez-Dans J. ESA CCI ECV Fire Disturbance: D2.1.3 Algorithm Theoretical Basis Document-MODIS, version 1.1. https://www.esa-fire-cci.org/documents, 2018.

Roy, D., Frost, P., Justice, C., Landmann, T., Le Roux, J., Gumbo, K., Makungwa, S., Dunham, K., Du Toit, R., and Mhwandagara, K.: The Southern Africa Fire Network (SAFNet) regional burned-area product-validation protocol, International Journal of Remote Sensing, 26, 4265-4292, 2005.

Schepers, L., Haest, B., Veraverbeke, S., Spanhove, T., Vanden Borre, J., and Goossens, R.: BA Detection and Burn Severity Assessment of a Heathland Fire in Belgium Using Airborne Imaging Spectroscopy (APEX). Remote Sensing, 6(3), 1803–1826. doi:10.3390/rs6031803, 2014.

Tum, M., Günther, K., Böttcher, M., Baret, F., Bittner, M., Brockmann, C., and Weiss, M.: Global Gap-Free MERIS LAI Time Series (2002–2012). Remote Sensing, 8(1), 69. doi: 10.3390/rs8010069, 2016.

van der Werf, G. R., Randerson, J. T., Giglio, L., van Leeuwen, T. T., Chen, Y., Rogers, B. M., Mu, M., van Marle, M. J. E., Morton, D. C., Collatz, G. J., Yokelson, R. J., and Kasibhatla, P. S.: Global fire emissions estimates during 1997–2016, Earth Syst. Sci. Data, 9, 697-720, https://doi.org/10.5194/essd-9-697-2017, 2017.

Zeng, J., Li, Z., Chen, Q., Bi, H., Qiu, J., and Zou, P.: Evaluation of remotely sensed and reanalysis soil moisture products over the Tibetan Plateau using in-situ observations. Remote Sens. Environ. 163, 91–110, 2015.

Annex 1: Acronyms and abbreviations

AUST	Australia
AVHRR	Advanced Very High Resolution Radiometer
BA	Burned Area
BOAS	Boreal Asia
BONA	Boreal North America
CCI	Climate Change Initiative
CEAM	Central America
CEAS	Central Asia
CV	Coefficient of Variation
DoB	Date of Burn
ECV	Essential Climate Variables
EQAS	Equatorial Asia
ESA	European Space Agency
EURO	Europe
FOA	Fraction of observed area
FRE	Fire Radiative Energy
GFED	Global Fire Emissions Database
GIO-GL1	Gio Global Land Component Lot1
GPWv4	Gridded Population of the World, Version 4
LTDR	Long Term Data Record
MAE	Mean Absolute Error
MCD45A1	MODIS/Terra+Aqua Burned Area Monthly L3 Global 500m SIN Grid
MCD64A1	MODIS Direct Broadcast Monthly Burned Area Product
MERIS	Medium Resolution Imaging Spectrometer
MIDE	Middle East
MODIS	Moderate Resolution Imaging Spectroradiometer
NHAF	Northern Hemisphere Africa
NHSA	Northern Hemisphere South America
PIR	Product Intercomparison Report
SEAS	Southern Asia
SHAF	Southern Hemisphere Africa
SHSA	Southern Hemisphere South America
SPOT-VGT	Satellite pour l'observation de la terre Vegetation
TENA	Temperate North America

Annex 2: GIO-GL1 product analysis

GIO-GL1 deviates from all other BA products in terms of the contribution of individual geographical regions to global BA. For example, in GIO-GL1, BA in Africa contributes 46% to global BA while in all seven BA products included into the core product intercomparison study (comparison of Figure 24 with Figure 4), the contribution of Africa is substantially larger, namely between 68 and 75% (Table 5). Of all BA products, GIO-GL1 yields by far the lowest total global BA.

The GIO-GL1 global estimate is by 33 to 51% lower than that of the other products. The estimate for the African continent is even 57 to 68% lower. Reversely, for BONA, MIDE and TENA, GIO-GL1 yields substantially higher estimates (5 to 27 times as high) as any other product in these regions.

Of all BA products, GIO-GL1 shows the lowest agreement with other products in terms of relative contribution of GFED regions to global total BA (Table 5b).

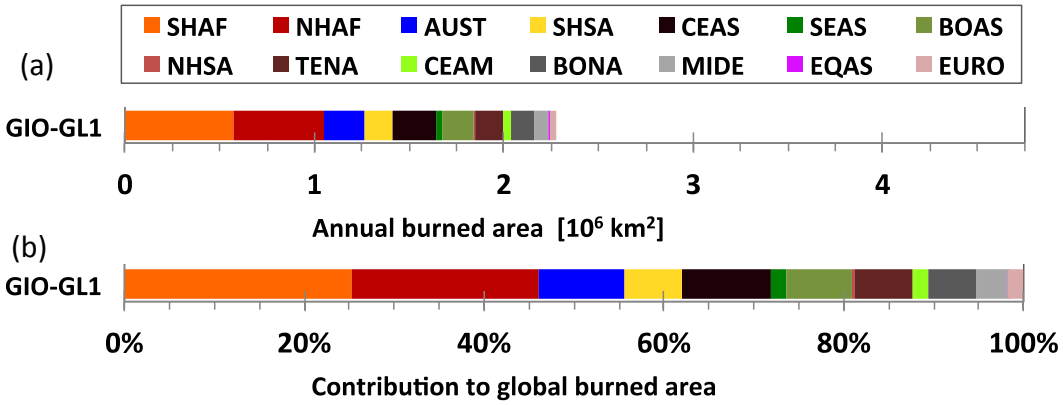

Figure 24: (a) Mean annual BA totals by GFED regions (period 2005 to 2011) in the GIO-GL1 product. (b) same as (a), but as relative contributions to global total BA. This figure compares to Figure 4.

Table 5: (a) Mean annual global BA (across 2005 to 2011) in the GIO-GL1 product and relative contribution by GFED geographical regions. This table compares to ¡Error! No se encuentra el origen de la referencia.. **(b) Mean absolute difference (MD) in regional contributions (across 2005 to 2011) to global BA with respect to different product pairs. This table compares to**

	Product	GIO-GL1
(a)	BA (mio km²)	2.28
	% burned by region	
	SHAF	25.2
	NHAF	20.9
	AUST	9.5
	SHSA	6.5
	CEAS	9.9
	SEAS	1.7
	BOAS	7.2
	NHSA	0.37
	TENA	6.4
	CEAM	1.8
	BONA	5.2
	MIDE	3.5
	EQAS	0.06
	EURO	1.7

(b) MD	GIO-GL1
FireCCI50	3.8%
FireCCI41	4.6%
MCD64C6	3.8%
MCD64C5	4.3%
GFED4s	4.0%
MCD45	4.0%
FireCCILT1	4.6%

In terms of rank order of continental contributions to global BA, GIO-GL1 strongly differs. North America, for example, ranks second while it has the sixth rank in all other BA products. Reversely, South America ranks sixth while it ranks third or fourth in all other products (Figure 25).

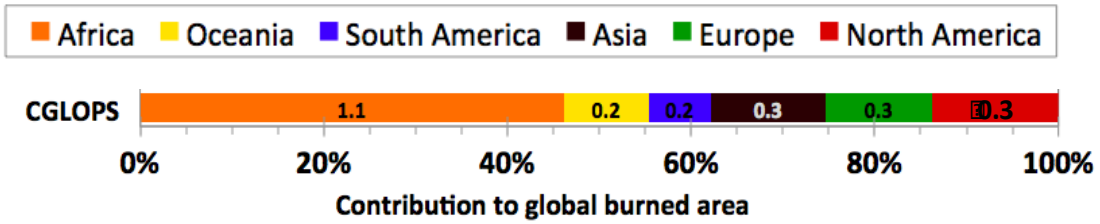

Figure 25: Continental contribution to global total BA (period 2005 to 2011) in the GIO-GL1 product The bars indicate the relative contribution while data labels in the bars provide the mean annual BA [in Mm^2]. This figure compares to Figure 3.